Validation of the TOLNet Lidars: The Southern California Ozone Observation Project (SCOOP)

Thierry Leblanc[1], Mark A. Brewer[1], Patrick S. Wang[1], Maria Jose Granados-Muñoz[1,2], Kevin B. Strawbridge[3], Michael Travis[3], Bernard Firanski[3], John T. Sullivan[4], Thomas J. McGee[4], Grant K. Sumnicht[5], Laurence W. Twigg[5], Timothy A. Berkoff[6], William Carrion[6], Guillaume Gronoff[6,7], Ali Aknan[6], Gao Chen[6], Raul J. Alvarez[8], Andrew O. Langford[8], Christoph J. Senff[9], Guillaume Kirgis[9], Matthew S. Johnson[10], Shi Kuang[11], and Michael J. Newchurch[11]

[1] Jet Propulsion Laboratory, California Institute of Technology, Wrightwood, CA 92397, USA
[2] Remote Sensing Laboratory/CommSensLab, Universitat Politècnica de Catalunya, Barcelona, Spain
[3] Air Quality Processes Research Section, Environment and Climate Change Canada, Toronto, ON, Canada
[4] NASA Goddard Space Flight Center, Greenbelt, MD, USA
[5] Science Systems and Applications Inc., Lanham, MD, USA
[6] NASA Langley Research Center, Hampton, VA, USA
[7] Science Systems and Applications Inc, Hampton, VA, USA
[8] NOAA Earth System Research Laboratory (ESRL) Chemical Sciences Division, Boulder, CO, USA
[9] University of Colorado Cooperative Institute for Research in Environmental Sciences (CIRES) at the NOAA Earth System Research Laboratory (ESRL) Chemical Sciences Division, Boulder, CO, USA
[10] NASA Ames Research Center, Moffett Field, CA, USA
[11] University of Alabama in Huntsville, AL, USA

Correspondence to: Thierry Leblanc (thierry.leblanc@jpl.nasa.gov)

Abstract. The North-America-based Tropospheric Ozone Lidar Network (TOLNet) was recently established to provide high spatio-temporal vertical profiles of ozone, to better understand physical processes driving tropospheric ozone variability, and to validate the tropospheric ozone measurements of upcoming space-borne missions such as Tropospheric Emissions: Monitoring Pollution (TEMPO). The network currently comprises six tropospheric ozone lidars, four of which are mobile instruments deploying to the field a few times per year, based on campaign and science needs. In August 2016, all four mobile TOLNet lidars were brought to the fixed TOLNet site of JPL-Table Mountain Facility for the one-week-long Southern California Ozone Observation Project (SCOOP). This intercomparison campaign, which included 400 hours of lidar measurements and 18 ozonesondes launches, allowed for the unprecedented simultaneous validation of five of the six TOLNet lidars. For measurements between 3 and 10 km above sea level, a mean difference of 0.7 ppbv (1.7%), with a root-mean-square deviation of 1.6 ppbv or 2.4% was found between the lidars and ozonesondes, which is well within the combined uncertainties of the two measurement techniques. The few minor differences identified were typically associated with the known limitations of the lidars at the profiles altitude extremes (i.e., first 1 km above ground and at the instruments highest retrievable altitude). As part of a large homogenization and quality control effort within the network, many aspects of the TOLNet in-house data processing algorithms were also standardized and validated. This thorough validation of both the

measurements and retrievals builds confidence in the high quality and reliability of the TOLNet ozone lidar profiles for many years to come, making TOLNet a valuable ground-based reference network for tropospheric ozone profiling.

5   1 Introduction

Although vital in the stratosphere, ozone has long been recognized as an air pollutant near the Earth's surface, causing health problems for humans and vegetation at high concentration (World Health Organization, 2003). Tropospheric ozone is also a short-lived greenhouse gas impacting climate, contributing to the Earth's global warming (IPCC, 2013). Despite significant regulatory efforts and pollution-control programs developed over the past 20 years in the most densely-populated regions of 10 the globe (e.g., Europe, North America and more recently Asia), recent reports of continuing free tropospheric ozone increases, for example in the Western United States (Cooper et al., 2012; Granados-Muñoz and Leblanc, 2016), have triggered the need to enhance our tropospheric ozone observation capabilities. In this context, the North American-based Tropospheric Ozone Lidar Network (TOLNet, https://www-air.larc.nasa.gov/missions/TOLNet/) was recently established to provide high spatio-temporal observations of tropospheric ozone to 1) better understand physical processes driving the ozone 15 budget in various meteorological and environmental conditions, and 2) validate the tropospheric ozone measurements of upcoming space-borne missions such as TEMPO (Tropospheric Emissions: Monitoring of POllution, http://tempo.si.edu) (Zoogman et al., 2014; Johnson et al., 2018) or TROPOMI (TROPOspheric Monitoring Instrument, http://www.tropomi.eu/). As of 2018, the network comprises six high-capability Ozone Differential Absorption Lidars (DIAL), namely the Canadian-based Autonomous Mobile Ozone Lidar for Tropospheric Experiments (AMOLITE) 20 (Strawbridge et al., 2018), the National Aeronautics and Space Administration (NASA) Langley Mobile Ozone Lidar (LMOL) (De Young et al., 2017), the University of Alabama in Huntsville Rocket-city O_3 Quality Evaluation in the Troposphere lidar (RO$_3$QET) (Kuang et al., 2013), the JPL-Table Mountain Tropospheric Ozone Lidar (TMTOL) (McDermid et al., 2002), the National Oceanic and Atmospheric Administration (NOAA) Tunable Optical Profiler for Aerosol and oZone Lidar (TOPAZ) (Alvarez et al., 2011), and the NASA Goddard Space Flight Center mobile Tropospheric 25 Ozone Lidar (TROPOZ) (Sullivan et al., 2014). Four of these lidars (AMOLITE, LMOL, TOPAZ, and TROPOZ) are mobile systems for deployment at remote locations, depending on field campaign and science needs of the moment. The remaining two systems operate at fixed locations, the RO$_3$QET system located at the University of Alabama in Huntsville Campus, and the TMTOL system being located at the JPL-Table Mountain Facility (TMF) in Southern California.

In August 2016, taking advantage of a favorable field deployment calendar, all four TOLNet mobile lidars were brought to 30 the fixed TOLNet site of JPL-TMF for a one-week-long intercomparison campaign that allowed for the unprecedented, simultaneous validation of five of the six TOLNet lidars: the Southern California Ozone Observation Project (SCOOP). As part of the international Network for the Detection of Atmospheric Composition Change (NDACC) (De Mazière et al.,

2018), TMF is a well-recognized research facility for the validation of atmospheric remote sensing instrumentation (e.g., Leblanc et al., 2011; McDermid et al., 1995). In addition to its three NDACC lidars (one of them being TMTOL), the facility hosts pressure-temperature-humidity (PTU) sonde and ozonesonde launch systems, radiometers, spectrometers, and surface composition and weather instruments. In support of the SCOOP campaign, several surface ozone monitoring instruments were operated at the site 24/7, and 18 ozonesondes were launched, and used as a reference transfer for the validation of the TOLNet lidars.

Prior to this study, three of the TOLNet lidars including TOPAZ, TROPOZ, and LMOL participated in Deriving Information on Surface Conditions from COlumn and VERtically-Air Quality (DISCOVER-AQ) field campaign in Colorado in 2014 showing mean relative difference within 4% between these three lidars (Wang et al., 2017). However, after the DISOVER-AQ campaign, the TOPAZ and LMOL systems have experienced significant hardware upgrades resulting in better stability, higher precision, and much higher measurable altitudes.

This paper reviews the TOLNet lidar measurement and retrieval validation efforts undergone prior, during and immediately after the SCOOP campaign, which eventually led to the current routine production of homogeneous, quality-controlled ozone profiles from the AMOLITE, LMOL, TMTOL, TOPAZ and TROPOZ lidars. After a brief technical description of the participating TOLNet lidar instruments (section 2), the campaign operational details relevant to the validation of the lidars are reviewed (section 3). The validation of the TOLNet data processing algorithms is summarized in section 4. The blind intercomparison of the lidar and ozonesonde measurements during SCOOP is presented in section 5. This dual algorithm/measurement validation approach allows the separation of ozone biases owed to the data processing on one hand and to the measurement itself on the other hand. The final outcome is presented in section 6, and all the results are summarized in section 7. Conclusions are provided in section 8 together with a brief discussion on the possible avenues of future TOLNet development.

2 Participating TOLNet Lidar and other Instruments

Five of the six TOLNet lidars participated in the SCOOP campaign. During the few months preceding the campaign, some of these lidars had undergone a few instrument configuration changes and further validation therefore turned out to be timely. By the end of the SCOOP campaign, and as will be demonstrated in this article, all five lidar systems proved to provide excellent quality ozone profiles, and their performance during the SCOOP campaign is believed to remain stable for years to come. Each instrument is briefly described below. Key transmitter specifications for all ozone lidar systems are compiled in Table 1, key receiver specifications in Table 2, and key data acquisition settings in Table 3.

2.1 The Canadian AMOLITE Lidar

The Autonomous Mobile Ozone Lidar Instrument for Tropospheric Experiments (AMOLITE) was designed and built by Environment and Climate Change Canada (Strawbridge et al., 2018), leveraging on a decade-long past experience of

building autonomous mobile aerosol lidars (Strawbridge, 2013). Space in the 2.1 x 4.3 m (WxL) trailer was optimized to house two dual-laser lidars, one dedicated to the measurement of tropospheric ozone, and the other one to the measurement of aerosol and water vapour. Weather instruments (including a precipitation sensor), radar interlock, and sophisticated heating/cooling systems are among the many safety components necessary to ensure continuous, unattended, remote

5   operations. Each of the two lidar systems comprises dual lasers to help minimize data gaps in case of equipment failures.

The ozone system, which produced all AMOLITE ozone profiles presented here, comprises two Nd:YAG lasers producing 45 mJ per pulse at 266 nm and 20 Hz. The 266 nm beam is sent through a 1-m-long cell filled with CO_2 (Nakazato et al., 2007) for Raman-shifting, then directed vertically by a steering mirror, which can be remotely controlled for beam-telescope re-alignment. Backscattered light is collected on a 35-cm-diameter Schmidt-Cassegrain telescope and spectrally separated to

10   two photomultiplier tubes (PMT) collecting the light at the Raman-shifted wavelengths of 287 nm and 299 nm, which corresponds to the second and third Stokes lines of CO_2 respectively. The PMT signals are time-sampled at 25 ns intervals (i.e., 3.75 m resolution) by a Licel analog/photon counting transient recorder. During night time and for a 5-minute integration time, the combination of laser power, telescope size, and receiver efficiency allows for ozone measurements between 400 m above ground and 15 km altitude. AMOLITE operates 24 hours a day, seven days a week except during

15   precipitation. The system is operated remotely and the data are updated hourly to a website providing near real-time capability.

2.2 The NASA-LaRC LMOL Lidar

The Langley Mobile Ozone Lidar (LMOL) is a ground-based tropospheric profiling ozone lidar system housed in a mobile trailer that has participated in air quality studies since 2014 (Young et al., 2017). Like the other TOLNet lidar systems,

20   LMOL relies on ultra-violet pulsed laser source that produces two wavelengths allowing for calculation of O3 concentration profiles from atmospheric differential absorption (Browell et al., 1985). The laser transmitter is similar to the NOAA system and consists of a custom built Ce:LiCAF tunable UV oscillator that is pumped by a frequency doubled (527 nm) commercially available Nd:YLF laser operating at a 1 kHz repetition rate. For the multi-wavelength UV pulse generation, a high-reflectivity rear cavity mirror mounted on a servo controlled galvanometer motor allows for rapid tuning of the

25   Ce:LiCAF output between two wavelengths suitable for ozone DIAL measurements. During the SCOOP campaign the On-line/Off-line DIAL wavelengths 287.1 and 292.7 were used and remained stable for the duration of the campaign. Light was transmitted in a zenith direction into the atmosphere from a hatch on the trailer roof at ~ 100 uJ/pulse, alternating pulse-to-pulse between the On-line/Off-line wavelengths (500 Hz each).

Backscattered light from the atmosphere was collected by a co-aligned 40 cm diameter fibre-coupled Newtonian telescope

30   with a 1.4 mrad filed-of-view, providing measurements from 0.6-8 km in altitude. The fibre output from the 40 cm telescope was connected to a light-tight enclosure containing a collimating optic, a pair of UV band-pass filters in series (280–295 nm spectral window) that were integrated with Hamamatsu photo-multiplier tube (PMT) R7400-U03 detector. The PMT output was connected to a single-channel, 12-bit Licel data system that provided simultaneous analog and photon counting outputs.

The Licel system memory was synchronously gated with the alternating wavelength pulses, to separately capture profiles for the On-Line/Off-line data and subsequently recorded by the instrument computer system for processing of raw signals into calibrated ozone profiles.

The processing of profiles was implemented following the standard DIAL technique (Browell et al., 1985). Raw signals both analog and photon counting are background subtracted and range-squared before applying a single-pass Savitzky-Golay filter (Leblanc et al., 2016a, and references therein); the more points used in the filter, the lower the resolution. Analog and photon-count channels are merged together to provide a single optimized profile for range and signal-to-noise performance (Leblanc et al., 2016b; Zhang et al., 2014; Newsom et al., 2009). Ozone cross sections along with pressure and temperature information are used as part of the filter process to extract ozone mixing ratio as a function of altitude. The process is repeated for each new profile on a 5-10 minute temporal averaged basis, to provide a continuous curtain display on the evolution of ozone vertical distribution during the course of a day. From a data analysis perspective, the more the data are averaged vertically, the lower the noise, but at the expense of the vertical resolution. A real-time data display was also available, allowing for display of the system generated ozone curtain profiles as are collected, for immediate feedback on atmospheric observations. This display was also linked over the internet, and could be remotely monitored, along with other system parameters.

It is important to note that LMOL was originally configured to only collect data in the lower troposphere and hence the data system range configuration was limited to 15 km. The background subtraction value is determined from the last ~2 km in range (no pre-pulse bins are available). Ordinarily this does not pose a problem, however the SCOOP type analyses can reveal a bias error due in LMOL to residual laser light being captured in the range bins used for background value determination. This is particularly true for extended temporal averaging (> 30 minutes) at high-altitude (> 9 km) at night-time, where this can result in systematic error > 10%. Since the SCOOP campaign, a new data system card was purchased and data system configuration implemented that eliminates these effects.

Since the SCOOP campaign, there are a number of instrument improvements that have been implemented that further enhance the capabilities of the LMOL system. These include implementation of a second, smaller diameter wide-field telescope to allow measurements in the 120-1000 meter altitude range (Farris et al., 2018; Gronoff et al., 2018), replacement of the outdated PMT with Hamamatsu model R9880U-113, and a new transmit configuration and roof window system to enable continuous unattended measurements. Since SCOOP, the LMOL system has successfully participated in three additional field deployments.

2.3 The NASA-JPL TMTOL lidar

The JPL-TMF tropospheric ozone lidar (TMTOL) is the third of four lidars designed at JPL for the long-term monitoring of atmospheric composition, thus contributing to the international network NDACC since 1999 (McDermid et al., 2002). Over the course of nearly 20 years, the system went through several hardware and operational modifications.

The emitter comprises a quadrupled Nd:YAG laser producing two beams of approximately 1 W each at 266 nm, at a repetition rate of 30 Hz. Each beam is sent through a Raman cell, one cell filled with Hydrogen and the other with Deuterium, to shift the wavelength to 299.1 nm and 288.9 nm respectively. The two beams are expanded five times to reduce their divergence (to less than 1 mrad), and to make them eye-safe as soon as they are transmitted outside the lidar building.

5 The optical receiver comprises a large Newtonian telescope (91 cm diameter, 2.4 m focal length) coupled with a dual optical fibre sending the lidar high-intensity returns to a polychromator. Two small telescopes (5 cm diameter), each aligned to one of the transmitted beams, are used to collect the near-range (low-intensity) signals. For each small telescope the light is focused at the entrance of an optical fibre and sent to the polychromator. This latter comprises four independent optical paths determined by the position of the fibres' output, corresponding to two high-intensity and two low-intensity channels. Until

10 2012, a mechanical chopper with 4 slits coinciding with the position of the fibres' outputs blocked the transmission of the strongest returns (lowest 1 km) from the large telescope fibres. Since 2012, the chopper wheel has been kept in a fixed open position allowing to transmit the returns from all altitudes for all four fibres' outputs. The light output from each fibre is transmitted through a dichroic beam splitter reflecting shorter wavelengths (Hartley band), a collimating lens, an interference filter (2 nm Full-Width-at-Half-Maximum (FWHM) centred at 289 nm or 299 nm, depending on the fibre considered) and a

15 focusing lens, before it reaches the surface of a photomultiplier tube (Hamamatsu H5783P-06). Although of old age, these photomultipliers have proved to be very reliable on the long-term, with minimal signal-induce noise despite the presence of high intensity returns.

The data acquisition system includes four joint analog-photon-counting Transient Recorders (Licel) allowing a vertical sampling of 7.5 m between the ground and 60 km altitude. The 16-bit analog signals are not used in the current SCOOP data

20 analysis, and only the results coming from the photon-counting channels are shown here.

Before data acquisition, the two emitted beams are aligned to the large telescope mirror axis using a computer-controlled motion controller and actuators changing the orientation of the two transmitting mirrors. When properly aligned, the low-intensity channels can be used down to an altitude range of 600 m above ground, i.e., 2.9 km above sea level (a.s.l.).

During the SCOOP campaign the lidar typical altitude range after combining the low- and high-intensity channels extends

25 from 2.9 km to 15 km a.s.l.. During the night, the top altitude typically reaches 18 km for a 30-min averaged profile. It is extended to 25 km by adding another DIAL pair of channels using the 299 nm high-intensity signal of TMTOL as the absorbed signal, and the low-intensity 355 nm signal of the co-located NDACC Water Vapour Raman lidar as the non-absorbed signal.

In routine operation mode, the raw signals are saved every 5 minutes. They are then averaged to the desired vertical and

30 temporal resolutions based on the science needs. For NDACC, the lidar routinely operates 2 hours per night, 4-5 nights per week, year-round. The two-hour averaged (night-time-only) ozone profiles are archived systematically at the NDACC Data Archive Centre, forming a long-term dataset of more than 2000 profiles (3-25 km) since 1999. For the SCOOP campaign, the lidar operation was extended to all times of the day, with ozone profiles reaching a 8-10 km top altitude during the brightest hours of the day, and 15-25 km top altitude at night-time. During the SCOOP campaign, the only hardware

configuration difference with the description of McDermid et al. (2002) is the discontinued use of the chopper and the newer
Licel system.

5 **2.4 The NOAA TOPAZ Lidar**

The Tunable Optical Profiler for Aerosol and oZone (TOPAZ) lidar is a compact differential absorption lidar for
measurement of ozone concentrations and aerosol backscatter in the lower troposphere that was originally designed (2006)
as a nadir-viewing airborne instrument for the NOAA Twin Otter aircraft (Alvarez et al., 2011). The airborne system was
deployed in the 2006 TexAQS (Senff, 2010) and 2010 CalNex (Langford et al., 2012) campaigns before being converted for
10 zenith-viewing ground-based operation from a medium box truck in 2012 with an external turning mirror for slant path
measurements within the lowest levels of the boundary layer. The truck-based system has been deployed to several field
campaigns including the 2013 Las Vegas Ozone Study (Langford et al., 2015).

Like the LMOL system, the TOPAZ transmitter is built on a rapidly-tunable (285 – 310 nm), all-solid-state Ce:LiCAF laser
pumped by a frequency-quadrupled, diode-pumped Nd:YLF laser. The TOPAZ laser also operates at high pulse repetition
15 rates (1000 Hz) and low pulse energy (average of 50 μJ/pulse, with 100 ns pulse-width), but sequentially tunes between 3
different wavelengths giving an effective pulse repetition rate of 333 Hz. Typical operation is with laser pulses at ~287, 290,
and 293 nm emitted sequentially and transmitted coaxially with the receiver telescope. The receiver uses a 0.5 m diameter
Newtonian telescope to direct the backscattered lidar signal to two photomultiplier (PMT) detectors with wide/narrow
(3.0/1.5 mrad) field of view for a near-field/far-field channel with a power split of 10%/90% respectively. The upward-
20 looking telescope is located beneath a port in the truck roof that is capped by a large computer-driven mirror that can direct
the coaxial transmitted and return beams along angles ranging from -5 to 30 degrees elevation. The turning mirror can also
move out of the beam path to allow vertical data collection. Measurements taken at several angles (typically, 2, 6, 20, and 90
degrees elevation), along with an assumption of horizontal homogeneity, allow the combined profiles to extend from near
ground level to the maximum vertical range (~5-6 km above ground level (AGL) during the day and ~8-9 km AGL at night).
25 The scanner azimuth direction is fixed but adjustable according to the site and experiment requirements. A recent (2016)
upgrade from the original field-programmable-gate-array-based data acquisition system developed for aircraft operation to a
new Licel hybrid data collection system has been implemented which includes both analog-mode (16 bit, 20 MS/s) and
photon counting (to 250 MHz) detection along with new PMTs. This upgrade has significantly improved the useful signal
range as described above. The data collection system accumulates signals over 1 second intervals and records the raw data to
30 disk while a separate processor carries out computation of the ozone and aerosol profiles at the completion of each scanner
sequence (typically 5-8 minutes).

2.5 The NASA-GSFC TROPOZ Lidar

The NASA Goddard Space Flights Center TROPospheric OZone Differential Absorption Lidar (TROPOZ) was designed in 2013 and installed in a 13 m transportable trailer (Sullivan et al., 2014). It has been routinely taking measurements in the Baltimore-Washington D.C. region since Fall of 2013. Its configuration is similar to the JPL TMTOL lidar. A quadrupled

5 Nd:YAG laser transmits 266 nm at 50 Hz into two 1.8-m-long cells filled with Deuterium and Hydrogen to Raman-shift the 266 nm wavelength to 289 and 299 nm.

The receiver comprises a 45-cm-diameter Newtonian telescope, four 2.5-cm refracting telescopes, a set of beam splitters, 289 nm and 299 nm interference filters, neutral density filters, and PMTs, allow all altitudes between 400 m above ground and 12 km to be covered. Signals from the PMTs are sampled at 50 ns intervals (7.5 m) by transient recorders operating in

10 analog and photon counting modes, and the data is typically recorded every 1 minute.

Since its inception, TROPOZ has been deployed to several field campaigns, including NASA's 2014 DISCOVER-AQ campaign (Sullivan et al., 2016) and the international KORUS-AQ Campaign (Korea-US Air Quality) in 2016 (Sullivan et al., 2017).

3 Review of the SCOOP Campaign Schedule and Logistics

15 ### 3.1 Lidar instruments deployment

As mentioned earlier, the planning of the SCOOP campaign leveraged from a favourable field deployment calendar of two of the four mobile TOLNet lidars. In early August 2016, the GSFC-based TROPOZ lidar was in transit back from the KORUS-AQ campaign in South Korea, and the NOAA-Boulder-based TOPAZ lidar was in transit back from the CABOTS campaign in the California Central Valley (Langford et al., submitted, 2018). The other two mobile lidars, AMOLITE and

20 LMOL, were brought from their respective home bases, i.e., Ontario, Canada and Hampton, VA, respectively. All lidar systems were ready and operational for the official kick-off of the campaign on August 11, 2016 (UT). The campaign was expected to finish on August 17 (UT), but a local wild fire triggered a one-day premature end to the campaign due to the mandatory evacuation of TMF. The SCOOP campaign therefore officially ended on August 16, 2016 at 2300 UT.

In order to optimize the measurements' simultaneity and co-location, two mobile lidars (TOPAZ and TROPOZ) were

25 deployed at the TMF core facility (2285-m a.s.l.) next to the JPL lidar building TM-21 (where TMTOL operates), and the other two mobile lidars (AMOLITE and LMOL) were deployed at the TM-2 Facility (2270-m a.s.l.), an annex to TMF located approximately 400 meters east-southeast of TM-21. This deployment configuration allowed the LMOL and AMOLITE lidars to operate next to each other (distance of 20 meters between the two systems) without cross-talk, and allowed LMOL to operate simultaneously with TOPAZ without cross-talk despite similar wavelengths. At the TM-21

30 location, the TOPAZ system operating at the highest frequency (1000 Hz) provided a master trigger to the TROPOZ (50 Hz) and TMTOL (30 Hz) systems, allowing full synchronization and simultaneous operations of the 3 systems without cross-

talk. Although cross-talk was avoided, spurious electronic interference in the TROPOZ and TMTOL signals occasionally occurred, partly due to a defective grounding of a TOPAZ subsystem, and partly due to the poor quality and extended length of trigger cables feeding TMTOL for the occasion. These complications caused the TOPAZ and TMTOL systems to miss a few hours of measurement and a couple of ozonesonde launches.

3.2 Lidars operation Schedule

The operational schedule of the SCOOP campaign was designed to spread the lidar measurements over all times of the day and night, over the course of one week. The AMOLITE lidar is automated and acquired measurements nearly 24 hours a day, 7 days a week. The other four lidars followed a pre-defined incremental measurement schedule, with more hours each day as the campaign progressed:

- August 10-11 (UT): 2 hours, early night
- August 11-12 (UT): 6 hours spread from midday to evening/early night
- August 12-13 (UT): 8 hours spread from late night/early morning to midday
- August 13-14 (UT): 12 hours spread from midday to midnight
- August 14-15 (UT): Rest day
- August 15-16 (UT): 18 hours spread from late night/early morning to evening/early night
- August 16-17 (UT): 24 hours spread from midday to midday next day (truncated by evacuation)

The above schedule defined the minimum requirement of SCOOP coordinated measurements. Most lidar instruments actually operated beyond the minimum requirement, leading to several hundreds of accumulated hours. Table 4 summarizes all lidars operating time over the SCOOP campaign period.

3.3 Other instrument operations during SCOOP

The JPL-TMF lidar group manages the operation of several ground balloon systems at TMF. In support of the SCOOP campaign, 17 Electrochemical Concentration Cell (ECC) ozonesondes (Komhyr, 1969; Smit et al., 2007) were launched from the site between August 10 and August 17. Another ozonesonde was launched 3 days prior to the official start of the campaign as a pre-campaign test-flight. The ozonesonde launch times were tailored to match the needs of the SCOOP campaign, with a number of launches ranging from a minimum of 1 launch per day on August 10 and August 11 (UT) to a maximum of six launches (one launch every 2 hours) on August 15-16 (UT). All the lidar measurements and launches planned on August 17 (UT) were cancelled due to the mandatory site evacuation order. Figure 1 summarizes the complete campaign schedule, including ozonesonde launches (labelled "ECC") and lidar operating times. In all upcoming figures, the ozonesonde data will be labelled "ECC".

Other in-situ or remote-sensing instruments operated during the campaign. An automated surface ozone analyser (ThermoFisher 49i) has been operating continuously at TMF since 2013. Several similar surface ozone instruments were also deployed as part of the TOLNet mobile lidars' added instrumentation. The surface ozone data are typically used to infer

physically-meaningful correlation relations between the values measured by lidar at their lowermost boundary (usually 200-600 m above ground) and the surface.

The JPL-TMF lidar group operates two other lidars at TMF for NDACC. The water vapor Raman lidar (Leblanc et al., 2012) was operated on three nights during SCOOP (August 10, 12 16 UT), and the stratospheric ozone lidar just resumed
5 operations during SCOOP after several months break due to laser failure. No results from those lidars will be shown in this article, but it is expected that the measurements from these lidars will be used together with the SCOOP campaign results for upcoming science investigations.

3.4 Table Mountain Facility environmental and meteorological conditions during SCOOP

The JPL Table Mountain Facility (34.38ºN, 117.68ºW) is at the top of a ridge, on the north (Mohave Desert) side of the San
10 Gabriel Mountains, northeast of the Los Angeles Basin in Southern California. It is a high-elevation site (2285 m a.s.l.), above the planetary boundary layer in all seasons except late spring and summer. At the surface, the ozone diurnal cycle is typically similar to that observed in the nearby high-desert, and is less pronounced than in the urban, near-sea-level Los Angeles Basin. The high elevation of TMF guarantees clean, clear skies over most of the lidars' measuring range, although in summer, the site is embedded in the top 1 km of the planetary boundary layer. Cloud interference during the SCOOP
15 campaign remained minimal. Out of the 7 campaign days, mid-elevation, afternoon cumulus clouds (3-5 km altitude a.s.l.) appeared at three occasions, on August 12 between 10 am and 4 pm PDT, August 13 between 10 am and 6 pm PDT, and August 16 after 1 pm PDT. Scattered high clouds (altitude 8-12 km a.s.l.) passed over TMF during the night of August 11 (PDT) and in the evening of August 13 (PDT). These favourable weather conditions allowed the lidars to measure during more than 90% of the SCOOP-prescribed coordinated days and times mentioned earlier.
20 An example of a 20-hour-long measurement run by the JPL lidar TMTOL is shown in Fig. 2. This ozone curtain plot, obtained on August 14, is typical of what all five co-located lidars have been measuring day after day during the campaign (a 31-day-long streak by AMOLITE is shown at the end of this article). The lidar's maximum vertical range is limited to 8-9 km in the middle of the day (0800 UT to 1100 UT) but extends to 14-16 km at night-time for the 10-minutes profiles shown here. Ozone measured by six ozonesondes launched on that day is superimposed in the form of coloured rectangles. In most
25 cases, they are barely noticeable because of the excellent quantitative agreement between lidar and ozonesonde. On this particular day, a clear layer of high ozone mixing ratio (80-90 ppbv) is observed between 4 km and 7 km, reaching the ground in the evening. Figure 2 also highlights the high ozone temporal variability, observed for example, between 0000 and 0600 UT on Aug 15 near 6-7 km a.s.l. (ozone increase from 40 ppbv to 80 ppbv). This high geophysical variability cannot be ignored when comparing non-simultaneous measurements, and particular care, not only on co-location, but also simultaneity,
30 must be taken.

3.5 SCOOP Level 2 data: 30-minute lidar-ozonesonde-coincident profiles

Hundreds of hours of lidar measurements were obtained during SCOOP. However, in order to minimize biases due to geophysical variability (see previous paragraph), only simultaneous profiles were critically compared. The results presented hereafter therefore focus on the lidar measurements made simultaneously with the first 30-minutes of each SCOOP
5   ozonesonde flight (i.e., the tropospheric part of the flights). Furthermore, during the blind validation phase ("blind" refers to ozone profiles retrieved by the 5 lidar teams without prior knowledge of the ozonesonde and other lidars' profiles), all five TOLNet lidar groups were asked to produce ozone profiles with the same effective vertical resolution in order to minimize biases introduced by differing vertical smoothing applied to the raw lidar data. The 30-minute-averaged sonde-coincident lidar profiles with this prescribed SCOOP effective vertical resolution scheme will be referred to as "SCOOP Level 2" data
10   throughout the rest of this work. The prescribed SCOOP effective vertical resolution scheme is altitude-dependent, linearly increasing from 200 m at 2.7 km altitude a.s.l. to 1500 m at 8.1 km altitude a.s.l, and then fixed to 1500 m above that. The vertical resolution scheme is shown in Fig. 3, left panel. Quantitatively, this scheme was chosen to ensure that random noise in the ozone profiles from all five lidars remains small. It is conservative for the LMOL, AMOLITE, and TOPAZ lidars, which could have benefited from a higher vertical resolution, but it provides just enough smoothing for the TMTOL low-
15   intensity channels to avoid the presence of excessive random noise. Vertical smoothing was also applied to the ozonesonde profiles to mimic the SCOOP effective vertical resolution scheme used for the lidars. By default, the ozonesonde raw data are produced at 1-second (~5 meter) intervals but their effective vertical resolution is 100-120 m due to the sonde time-response of about 20 seconds (WMO, 2014). To account for the difference between the lidars typical vertical sampling resolution of a few meters and the 100-120 m vertical resolution of the sonde, the averaging kernels applied to the sonde
20   profiles to mimic the lidar's effective resolution are slightly different from those applied to the raw lidar signals. What counts in the end is not the averaging kernels themselves, but how these kernels translate in terms of effective resolution. The middle and right panels of Fig. 3 show a comparison of ozonesonde profiles at the raw vertical resolution and at the SCOOP vertical resolution. Differences of 20 ppb or more can be found for individual flights. When averaging profiles from all 17 SCOOP launches, the differences reach up to 5 ppbv (10%) at 9 km and above (not shown). Working with the same
25   effective vertical resolution for all lidars and all ozonesonde profiles therefore avoids the introduction of smoothing-induced differences of up to 5 ppbv, or 10%, in the SCOOP level 2 mean profile comparisons shown thereafter.

Because of the operational constraints of the lidars, not all instruments were fully operational during each SCOOP ozonesonde flight. Furthermore, mid-elevation clouds appeared during 4 of the 17 ozonesonde flights, impacting differently the ozone retrievals of the various lidars. As a result, the actual number of ozonesonde-lidar coincidences is not 17 for all
30   systems, and the list of launches used for the comparisons varies from one pair of instruments to another. Table 5 summarizes the coincidences used, instrument-by-instrument, to produce the SCOOP Level 2 data after operational and weather constraints were taken into account. Figure 4 illustrates the sampling bias issues caused by the coincidence heterogeneity. For each of the six panels (ozonesonde + 5 lidars), the flight numbers during which valid ozone measurements

were made are listed (different colour for each flight). From this figure and as anticipated from the high temporal variability observed in Fig. 2, it is clear that the mean ozone profiles computed using one-to-one instrument coincidences are expected to vary significantly. This is confirmed in Fig. 5, which shows the mean ozone profiles computed for AMOLITE (left panel) and LMOL (right panel) when measurements coincide with the other instruments. For example, the mean AMOLITE ozone

5   profile computed using all coincidences with TMTOL (blue curve) is significantly different from the mean AMOLITE ozone profile computed using all coincidences with TOPAZ (purple curve). To minimize the impact of this heterogeneity (and the underlying differences therefore introduced by geophysical variability), the differences between ozone and lidar were investigated in a statistical manner, using the ozonesonde as the reference transfer. This approach maximizes the number of coincidences between the ozonesondes and one given lidar, but prevents us from comparing all sondes and all lidars together

10   simultaneously.

SCOOP Level 2 data validation results are presented thereafter. As part of the overall TOLNet lidar validation efforts, both the measurements and the retrieval algorithms were actually validated. This two-fold approach allows, in theory, the separation of biases due exclusively to the experimental conditions and those due exclusively to the data processing algorithms. The next section focuses on the algorithm aspects.

15   **4 Standardization and Validation of the TOLNet Lidar Data Processing Algorithms**

As part of producing the best quality and most homogeneous ozone profile dataset possible, the TOLNet community has engaged in a large effort to standardize and validate all TOLNet in-house data processing algorithms. This process leveraged from similar work done within the NDACC lidar community a few years ago (Leblanc et al., 2016a; 2016b), and led to the full implementation of several standardized features within the TOLNet algorithms today.

20   **4.1 Use of simulated lidar signals and centralized data processing to validate the algorithms**

Each standardized feature of the algorithms was verified through a comprehensive algorithm validation exercise. The modus operandi of this exercise is as follows: 1) Consider "known" atmospheric conditions (density, temperature, ozone, and other chemical species), 2) Simulate raw lidar signals as if they were acquired in these atmospheric conditions by a specific TOLNet lidar (forward model), 3) Analyze the simulated signals using the TOLNet lidar in-house data processing algorithm

25   to be validated (inverse model), and 4) Compare the ozone profile retrieved by the in-house data processing algorithm with the original ozone profile used to simulate the signals. If the retrieved and original profiles differ significantly, the source of the difference is investigated, corrections to the algorithm are made wherever necessary, and steps 3 and 4 above are repeated, until both original and retrieved profiles match perfectly (except for very small differences due to numerical rounding errors). This approach is used not only to validate the retrieved ozone profiles, but also other products output by the

30   algorithms, for example, vertical resolution, uncertainty, etc..

An example of algorithm validation result, in the context of SCOOP, is provided in Fig. 6. The left panel of this figure shows a comparison between the original ozone profile used in the forward model (cyan curve) and the profile retrieved by the AMOLITE in-house data processor (red curve). In this example, the forward model used the atmospheric conditions (T, p, O3) of the SCOOP ozonesonde tm073 launched on August 10, 2016. The original profile is barely noticeable because the

5 agreement is excellent and the retrieved profile is just on top of it. The purpose of this particular simulation run was to validate the AMOLITE in-house retrieval in absence of smoothing, and therefore the raw lidar signals were simulated without detection noise. The increasing noise at the top of the red profile is not detection noise, but simply the result of rounding errors associated with the numerical digitization of the simulated raw lidar signals. The middle panel shows the difference (in %) between the AMOLITE in-house retrieved ozone profile and the original ozone profile. These results show

10 that the AMOLITE in-house data processing algorithm produces the correct profile (i.e., no bias), keeping in mind that the numerical rounding errors at the top are an artefact that does not exist with real measurements. As part of the complete validation process, the ozone profile retrieved by the AMOLITE in-house data processor was also compared to the ozone profile retrieved by the centralized data processing software GLASS (Global Lidar Analysis Software Suite) developed at JPL-TMF. The GLASS includes all the standardization features recommended within NDACC and prescribed for the

15 TOLNet data processing algorithms. It can therefore be used here as a reference transfer. The difference between the AMOLITE in-house and GLASS retrievals is shown on the right panel of Fig. 6 (green curve). Because the numerical rounding errors were propagated similarly through both the GLASS and the AMOLITE in-house data processor, a better agreement and reduced noise is found between the two retrieved ozone profiles, compared to the difference observed with the original profile.

20 As part of the TOLNet-wide algorithm validation efforts, simulation runs similar to the present example were performed for all TOLNet instruments, either before or after SCOOP (e.g., Sullivan et al., 2015). This comprehensive effort led to the full validation of the TOLNet in-house retrievals, and any ozone bias identified during SCOOP between sonde and lidar, or between lidar and lidar, should not be expected to originate from the data processing algorithms.

4.2 Standardized effective vertical resolution

25 In addition to the retrieved ozone profiles, an essential algorithm feature to validate is effective vertical resolution. The standardized definition used by all TOLNet lidar groups is the NDACC-standardized definition prescribed in (Leblanc et al., 2016a). Using this definition, the reported vertical resolution corresponds to the FWHM of the response to a finite impulse, namely, a Delta Function for smoothing filters and a Heaviside Step Function for derivative filters. In DIAL retrievals, vertical smoothing can be applied either to the raw lidar signals or to the retrieved ozone profiles, or to both, by using either

30 smoothing filters or derivative filters, hence the importance of using a standardized definition that is representative of a specific effective resolution. A validation example is provided in Fig. 7. The left panel shows the original simulated ozone profile used in the forward model (cyan curve), and the AMOLITE in-house-retrieved and GLASS-retrieved ozone profiles (red and blue curve, respectively). The simulated ozone profile is the same as in Fig. 6, i.e., taken from the SCOOP launch

tm073 on August 10, 2016. Both in-house and GLASS retrieved profiles are smoother than the original profile as they were both processed using the same SCOOP effective vertical resolution scheme introduced in section 3.5. The excellent agreement between the two retrieved profiles confirms that the AMOLITE in-house data processor applies the correct amount of smoothing, i.e., uses the correct definition of effective vertical resolution. The middle and right panels are similar

5   to the left panel, but for LMOL and TROPOZ. They are additional examples illustrating that the other TOLNet data processing algorithms were checked for computing a consistent effective vertical resolution.

4.3 Standardized uncertainty budget

The next major aspect of the TOLNet algorithms that was standardized and validated is the uncertainty budget. The AMOLITE, LMOL, TMTOL, and TROPOZ data processing algorithms were checked to ensure that their uncertainty budget

10   followed the NDACC recommendations on uncertainty provided in Leblanc et al. (2016b). No such check occurred for TOPAZ as no uncertainty estimates were provided with their SCOOP level 2 data. Figure 8 shows an example of the detailed uncertainty budget computed by the AMOLITE (top-left), LMOL (top-right), TMTOL (bottom left), and TROPOZ (bottom right) in-house algorithms (solid curves), compared to their equivalent computed by the GLASS (thick dash curves, similar hues). The uncertainty budget computed by the GLASS follows the NDACC recommendations, and can be used once again

15   as a reference transfer. The random component of total uncertainty comes essentially from detection noise (Poisson statistics). This term is represented in black/grey in Fig. 8. The ozone total systematic uncertainty component is a combination of propagated ozone absorption cross-section differential uncertainty (pink/purple), signal (PMT) saturation correction uncertainty (yellow/orange), background noise (skylight) correction uncertainty (blue/cyan), Rayleigh scattering cross-section uncertainty (green) and air density uncertainty (brown). Aerosol extinction and backscatter uncertainty is not

20   included in the present uncertainty budget, partly because its quantitative estimation is difficult and no standardized recommendation exists, and partly because the SCOOP measurements were made at Table Mountain Facility, a high-elevation site, i.e., mostly above the boundary layer, with little impact from aerosols. The ozone total uncertainty is the quadratic sum of all uncertainty components shown in Fig. 8. In this figure, the effect of transitioning between channels (ranges) of different intensity (near-field to far-field, low-intensity to high-intensity, analog-to-photon-counting, etc.) is

25   manifested by sharp or step-like vertical gradients of uncertainty.

When comparing the solid and dash curves of similar hue in Fig. 8, it is clear that all four in-house data processing algorithms (solid curves) follow closely the GLASS computation (dash curves). Note that for TMTOL, the in-house and GLASS computations are identical, so the solid and dash curves overlap perfectly. There are only two cases of disagreement, both of which can easily be explained. One case is the saturation correction uncertainty (yellow) for AMOLITE near 5 km

30   and TROPOZ near 6 km. The discrepancy is simply due to the fact that the GLASS algorithm does not combine the low and high intensity channels the same way the AMOLITE and TROPOZ in-house algorithms do. The other case of disagreement is for random uncertainty (black/grey curves) below 5 km for AMOLITE and below 4 km for TROPOZ. This is due to the fact that the GLASS does not compute random uncertainty for analog channels the same way the AMOLITE and TROPOZ

in-house data processors do. This result calls for further work needed on possible recommendations to standardize this particular aspect of the data processing, not only for random uncertainty, but for all components of uncertainty for analog signals.

Figure 8 also provides important insights on the relative magnitude of each uncertainty component contributing to the total
5   uncertainty, as a function of altitude, and depending on the instrument considered. For example, the ozone uncertainty owed to the absorption cross-section differential uncertainty (pink/purple curves) has a consistent behaviour across all instruments, with nearly-constant values of 2% (AMOLITE, TMTOL and TROPOZ), and 4% (LMOL) throughout the entire profile. As part of the algorithm standardization process, a common set of temperature- and wavelength-dependent ozone absorption cross-sections, and their uncertainty, was used. This dataset originates from the works of Daumont et al. (1992) and Malicet
10   et al. (1995) for the absorption cross-section values, and from Weber et al. (2016) for their uncertainty. The original dataset is interpolated every 0.01 nm between 260 nm and 320 nm, and every 0.1 K between from 160 K to 330 K, then written in a unique lookup table file to be read by the TOLNet data processing algorithms.

Similarly to absorption cross-section differential uncertainty, the ozone uncertainty components owed to molecular extinction correction uncertainty (green and brown curves) exhibit a consistent altitude dependence and magnitude for all
15   instruments. This is explained by the consistent use by all TOLNet lidar data processing algorithms, of the same source of ancillary temperature and density profiles (and their uncertainty) during SCOOP. In the case of the SCOOP Level 2 data, the temperature and pressure measurements from the InterMet PTU radiosondes coupled with the ozonesondes were used.

On the other hand, no obvious consistency is observed for the remaining ozone uncertainty components, namely the components owed to detection noise (black/grey curves), saturation correction (yellow/orange), and background noise
20   correction (blue/cyan). These components are indeed instrument-dependent and exhibit large differences, both in magnitude and shape. The different instrument characteristics and the different range combination options shows that there is not one simple characterization of uncertainty for the TOLNet ozone lidars, even though they all use a consistent uncertainty budget approach.

4.4 From data processing algorithm validation to ozone profile validation

25   The purpose of the data processing algorithm validation described above is to identify and/or characterize sources of bias that are not due to the measurements or instrument conditions, but instead, to the data processing algorithms. Through a few selected examples, it was shown that the in-house TOLNet data processing algorithms participating in SCOOP were validated. Any deviation observed during SCOOP between sonde and lidar, or between two lidars, that exceeds the differences observed at the conclusion of these algorithm validation efforts (typically 1%) should therefore be interpreted as
30   owing to the experimental conditions rather than the algorithms.

Despite the large efforts to standardize and validate the TOLNet data processing algorithms, there are still a few features that were not, or cannot be, standardized. Among them are the process of combining various intensity channels, the process of combining analog and photon-counting channels, and the method to correct or remove the influence of aerosol and clouds. In

particular, the method of combining various intensity channels to form a single profile depends strongly on the experimental configuration (i.e., how many channels are available, what are their wavelengths, and what are their intensities). In the next section, it will be shown that such experimental aspects actually can explain a large fraction of the differences observed between the various lidar measurements and their uncertainty during the SCOOP campaign.

5 **5 SCOOP Level 2 Data Comparisons**

5.1 One-on-one comparisons

One-on-one instrument intercomparison profiles are given in Fig. 9 for all 5 lidar instruments with respect to the ozonesondes. The left panels show the mean ozone profiles computed using all available one-on-one coincidences between ozonesonde (cyan curves) and lidar (from top to bottom: AMOLITE in red, LMOL in green, TMTOL in blue, TOPAZ in

10 purple, and TROPOZ in yellow). For each instrument, the thin dotted lines denote the ozone profiles +/-1-σ uncertainty. The middle and right panels show the ozone differences between lidar and ozonesonde in parts-per-billion (ppbv) and in percent (%) respectively, with the ozonesonde being the reference. The grey-shaded areas denote the combined total uncertainty (quadratic sum of each instruments' total uncertainty). No uncertainty estimate was given by the NOAA TOPAZ lidar group. The 4th row of Fig. 9 therefore includes the ozonesonde uncertainty only, which explains a smaller shaded area than for the

15 other rows. In view of the reported uncertainty estimates, no outstanding bias can be detected for any of the instruments compared here. The main result is a consistent agreement between sonde and lidar within the combined reported uncertainties, i.e., within 3-5 ppbv or 5-8%.

In order to identify possible biases owed to individual instruments, each lidar instrument was compared against all the others. The results are shown in Fig. 10. Each panel corresponds to a particular instrument, referenced at the top of each panel. The

20 coloured curves represent the mean ozone differences (in %) between the reference instrument and another instrument, computed using all available one-on-one coincidences for this particular pair of instruments. In each panel, the thick black curve represents the mean of all coloured curves. For a particular reference instrument, if the black curve displays outstanding features similar in shape and magnitude to features displayed by several coloured curves, then it is likely that these features are owed to the reference instrument. For example, the positive difference of 8-9% observed at around 5 km

25 altitude on the TMTOL panel (bottom row, middle panel) points out to a likely positive bias owed to TMTOL. Several other small biases can likewise be identified, more noticeably a -8% bias below 4 km for LMOL and TOPAZ, a +5% bias below 4 km for TROPOZ, a +10% bias at 3 km for TMTOL, and a reversed "S" shape from -5% at 5.5 km to +8% below 3 km for AMOLITE. The magnitude of these differences remains mostly within the reported uncertainties and the largest differences occur in regions known to be borderline in terms of validity of the lidar measurements (e.g., the profiles' lower boundary).

30 Interestingly, the ECC ozonesonde panel (top-left) exhibits the least (if any) significant feature, which seems to indicate that no bias arises from the sonde measurements, making the ozonesonde a suitable reference transfer for the SCOOP campaign. Noticeably, the number of coincidences used to compute the means for a particular pair of instruments varies with altitude

(not shown). This number maximizes in the 3-10 km altitude range (typically 13-16 coincidences), but quickly drops above 10 km and below 3 km, which contributes to increase the apparent magnitude of the differences in these regions. Finally, the potential loss of co-location in the upper troposphere between the drifting ozonesondes and the fixed lidars might also contribute to the slightly larger differences observed between sonde and lidar above 10 km.

5 Figure 11 is similar to the top-left panel of Fig. 10 (ref=ECC) but with the coincidences split by local time. The left panel shows the mean ozone difference between sonde and lidar computed for all five early night-time launches, and the right panel shows these differences for all four launches performed during mid-day (typically 11 am to 2 pm local time). Not surprisingly, the differences exhibit more noise due to a poorer sampling statistics, but also more noise at the top of the daytime profiles (lower signal-to-noise ratio due to daylight). However, no major mean bias stands out of either plot,

10 showing that both daytime and night-time profiles remain within the 7-8% total combined uncertainty shown in the earlier figures.

5.2 Uncertainties

The presence of five TOLNet lidars operating in identical conditions, and using common data processing options allowed for an objective assessment of their performance as a function of altitude range and time of the day, as well as an objective

15 comparison of their reported uncertainties.

Figure 12 shows two selected 30-minute ozone profiles (left panels) measured simultaneously by all five lidars in dark conditions (top) and in the brightest possible conditions (bottom), as well as their corresponding reported uncertainty expressed in parts-per-billion (middle panels) and percent (right panels). In the middle and right panels, the dotted curves denote the random component, the dash curves denote the systematic component, and the solid curves denote the total

20 uncertainty (computed as the quadratic sum of random and systematic components). The dotted curves on Fig. 12 therefore correspond to the black/grey curves shown in Fig. 8, and the dash curves in Fig. 12 represent the quadratic sum of all the systematic components displayed in Fig. 8.

The most striking feature in Fig. 12 is the difference in magnitude and shape between the uncertainty estimates computed for the various lidars. At night-time (top row), a similar dependence on altitude holds for most lidars, specifically, a nearly

25 constant total uncertainty of 1-4 ppbv (2-6%) from the lowest data point up to about 9 km, then an increase to about 5-10 ppbv (10-15%) at 12 km. The exception is TMTOL, with a total uncertainty of 5 ppbv (7%) below 5 km, followed by a decrease to 2 ppbv (3%) near 6-7 km, a wide peak at 6 ppbv (15%) near 8 km, and finally a decrease to 4 ppbv (8%) at 11 km, before increasing again like the other lidars. This difference between TMTOL and the other lidars can be explained by the use of 3 intensity ranges of very different characteristics: below 5 km, the TMTOL low-intensity channels were

30 unusually weak during SCOOP, and therefore yielded higher random uncertainty. The peak at 8 km comes from using a pair of very high-intensity channels, therefore leading to a higher estimate of saturation correction uncertainty (blue dash curve). This high-intensity pair is used for the purpose of extending the ozone profile well beyond the tropopause (typically 25 km) as part of the TMTOL's mandate to produce lower stratospheric ozone profiles for NDACC. On the night of August 16

(UT), as well as several other SCOOP nights, TMTOL encountered alignment and low signal-to-noise ratio issues on the low-intensity channels, which forced the transition from low-intensity to high-intensity channels at an unusually low altitude (i.e., 7-8 km instead of the usual 12-14 km used routinely between 1999 and 2015). This uncertainty peak of 15 % at 8 km is therefore not representative of TMTOL in normal conditions. Indeed, a few months after the SCOOP campaign, several

5   aging optics in the TMTOL transmitter and receiver were replaced, and the signal to noise ratio was significantly improved. The random uncertainty in the 3-12 km altitude range has since remained within the 7-8% range when using an effective vertical resolution and integration times similar to that of the present SCOOP Level 2 data. Finally, a brief, but sharp, increase of uncertainty is also observed for LMOL at 5-6 km (green curve), and to a lesser extent for TROPOZ at 4.5 km (pink curve). The increase is once again explained by the transition between the low-intensity range (analog channels) and

10   the high-intensity range (photon-counting channels).

In the bright conditions of mid-day (Fig. 12, bottom row), the altitude dependence of uncertainty is similar for all lidars, once again with the exception of TMTOL. Not surprisingly, uncertainty increases quickly for all lidars from the 1-4 ppbv (2-6%) values already noted at night-time, to 10 ppbv (15%) at around 9-10 km altitude, and >25 ppbv (>30%) at 12 km. The random component dominates, logically explained by high background noise associated with bright daylight. Once again,

15   TMTOL stands out with a higher random uncertainty than the other lidars below 5 km (5-8 ppbv, 10-12%), again associated with the low signal-to-noise ratio of the low-intensity channels during SCOOP.

6 SCOOP Level 3 Data and Final Validation Outcome

The blind phase of the TOLNet lidar validation efforts during the SCOOP campaign, together with a thorough TOLNet data processing algorithm validation exercise, represented key steps of the TOLNet lidars Quality Assessment and Quality

20   Control (QA/QC) process. For the AMOLITE, LMOL, and TMTOL lidars, these measurement and retrieval validation efforts led to the production of optimized ozone profiles, referred to as "SCOOP Level 3" data. With this data version, the ozone profiles' effective vertical resolution scheme is optimized and depends on the lidar considered (yet using the same NDACC-standardized definition). The new data version also incorporates some data processing refinements resulting from the algorithm validation exercise. For the TOPAZ and TROPOZ lidars, the in-house algorithm had been validated prior to

25   SCOOP, and the vertical resolution scheme used for the SCOOP Level 2 data was suitable enough to be kept as is. No data version change from level 2 to level 3 was therefore necessary.

Figure 13, top-row, shows the mean differences (left panel: in ppbv, middle panel: in percent) between the SCOOP Level 3 ozone lidar profiles and the ozonesonde profiles for all available one-on-one lidar-sonde coincidences (Level 2 data is shown for TROPOZ and TOPAZ). The right panel shows the number of coincidence pairs used for each instrument as a function of

30   altitude. The lidar-ozonesonde differences remain within +/-5 ppbv (8-10%), but this is now taking into account an additional smoothing error (the AMOLITE, LMOL and TMTOL effective vertical resolutions are no longer matching). Just like in Figs. 10 and 11, the thick black curve represents the mean of all the coloured lines present on the same plot. Taken as

a whole, the TOLNet lidars show outstanding agreement with the ECC ozonesondes, with an overall mean bias of 0.7 ppbv or 1.7% for the altitude range 3-10 km, and with a root-mean-square deviation of 1.6 ppbv or 2.4%.

The bottom row of Fig. 13 shows the mean of systematic (left panel) and random (middle panel) uncertainties associated with the coincidence pairs used to plot the ozone differences showed in the top row, as well as the reported effective vertical resolution (right panel). Table 6 summarizes the bias, precision and accuracy estimates of all the instruments, either taken separately or as a whole. The six panels of Fig. 13 altogether conclude the SCOOP validation efforts and summarize well the overall quality of the five TOLNet lidars that participated in the campaign. They provide, together with Table 6 and Fig. 10 (top-left panel), an excellent QA/QC review for the AMOLITE, LMOL, TMTOL, TOPAZ and TROPOZ lidar data, which can be used as a reference in future process studies and satellite validation efforts using these data.

7 Summary

Despite stringent air quality regulations put in place decades ago in many countries around the world, free tropospheric ozone increase has continued to increase in certain regions, including the Western United States. This increase contributed to the decision to expand tropospheric ozone observation capabilities in North America through the establishment of the TOLNet lidar network. In August 2016, five of the six TOLNet lidars (namely, AMOLITE, LMOL, TMTOL, TOPAZ, and TROPOZ) participated in the SCOOP intercomparison and validation campaign at the JPL-Table Mountain Facility in California. After significant efforts validating the TOLNet data processing algorithms, the SCOOP campaign provided an unprecedented opportunity to validate the simultaneous measurements of five co-located tropospheric ozone lidars.

Approximately 400 hours of lidar measurements were made and 17 ozonesondes were launched over the 1-week-long campaign, allowing for a thorough validation of the lidars. Over the range 3-10 km a.s.l., the mean difference between lidar and ozonesonde was found to be 0.7 ppbv (1.7%), with r.m.s. deviation of 1.6 ppbv or 2.4%, which is well within the combined reported uncertainties of lidar and sonde (Table 6). The rare and minor differences identified were typically associated with the known limitations of the lidars at the profiles boundaries, for example, errors associated with incomplete beam-telescope overlap and signal saturation at the bottom of the profiles (below 3-4 km a.s.l.), and random noise at the top of the profiles (above 10 km a.s.l.). Geophysical variability and the fact that the ozonesonde is no longer co-located with the lidars higher up, is also believed to contribute to some of the differences observed in the upper troposphere. Together with the measurements, many aspects of the data processing algorithms, such as ozone absorption cross-sections, the definition of effective vertical resolution, and the uncertainty budget, were standardized and validated. This thorough validation of both the measurements and retrievals gives high confidence in the quality and reliability of the TOLNet ozone lidar profiles.

8 Conclusion and Perspectives

After several years of instrumental development and optimization, the SCOOP campaign represents a turning point in the lifecycle of TOLNet. Upon their deployment in Southern California in August 2016, the participating TOLNet lidars had reached a mature stage of technical development. The 1-week-long SCOOP campaign represented the most comprehensive and rigorous TOLNet ozone lidar intercomparison yet. In particular, its focus on algorithm testing and homogenization ensures that TOLNet ozone lidar network data will be of the highest quality for years to come. The results of this campaign demonstrate the excellent accuracy of the tropospheric ozone lidar technique, which is expected to be used more intensively in the decades to come for high-vertical resolution profiling of tropospheric ozone.

One technical area towards which TOLNet is now thriving to work, is automated, autonomous field measurements. Figure 14 shows a 31-day ozone time-altitude cross-section obtained at TMF by the AMOLITE lidar during, and immediately after the SCOOP campaign. It illustrates nicely the full capability of an autonomous and automated tropospheric ozone lidar. Today, several other TOLNet lidars (e.g., TMTOL) are testing/implementing this new mode of operation. As technology improves and becomes more reliable and affordable, it is expected that most TOLNet instruments will converge towards autonomous operations. This mode of operation opens the door to advanced process studies (e.g., extended ozone diurnal variability studies), and will likely lead to the production of extensive ground-based reference datasets for process studies, as well as model and satellite validation. One example is the validation of the TROPOMI instrument on board the European satellite Sentinel 5P. For a given location, this instrument measures ozone at the same local time (1300 LT) every day. In 2017, the TMTOL lidar was upgraded to operate autonomously, upon demand. It was programmed to run automatically for one hour every day at approximately 1300 Local Time, and it has since acquired more than 150 correlative profiles for the validation of TROPOMI. Another application is the validation of the future NASA instrument TEMPO to be launched to a geostationary orbit in 2020/2021. For a given location in North America, this instrument will measure tropospheric ozone during daytime at 1-hour intervals with high horizontal resolution. The TMTOL lidar, and likely several other TOLNet lidars, will be programmed to measure for a few minutes every one hour during daytime, 7 days a week, which will provide a maximum number of correlative measurements with TEMPO, yet minimizing instrumental wear out.

Code availability

Questions pertaining to the methods and approaches used to perform the comparison and validation results presented here should be directed to the first author at thierry.leblanc@jpl.nasa.gov.

Data availability

All ozonesonde and ozone lidar profiles shown here, and obtained during SCOOP, are publicly available at the TOLNet website https://www-air.larc.nasa.gov/missions/TOLNet, or can be obtained by submitting a request to the participating lidar instrument PIs (authors).

5   **Acknowledgements**

The work described here was in part carried out at the Jet Propulsion Laboratory, California Institute of Technology, under agreements with the National Aeronautics and Space Administration. The Tropospheric Ozone Lidar Network and the SCOOP campaign acknowledge funding from the Tropospheric Chemistry Program of the NASA Earth Science and Division. The NOAA/ESRL lidar operations were also supported by the NOAA Climate Program Office, Atmospheric

10 Chemistry, Carbon Cycle, and Climate (AC4) Program. The views, opinions, and findings contained in this report are those of the author(s) and should not be construed as an official National Oceanic and Atmospheric Administration or U.S. Government position, policy, or decision. AMOLITE's participation was supported by the Environment and Climate Change Canada's Climate Change and Air Quality Program (CCAP) and the Joint Oil Sands Monitoring program (JOSM).

References

15 Alvarez, R. J., Senff, C. J., Langford, A. O., Weickmann, A. M., Law, D. C., Machol, J. L., Merritt, D. A., Marchbanks, R. D., Sandberg, S. P., Brewer, W. A., Hardesty, R. M., and Banta, R. M.: Development and Application of a Compact, Tunable, Solid-State Airborne Ozone Lidar System for Boundary Layer Profiling, J. Atmos. Ocean Tech., 28, 1258-1272, doi:10.1175/jtech-d-10-05044.1, 2011.

Browell, E. V., Ismail, S., and Shipley, S. T.: Ultraviolet DIAL measurements of O3 profiles in regions of spatially

20 inhomogeneous aerosols, Appl. Opt., 24, 2827-2836, doi:10.1364/ao.24.002827, 1985.

Cooper, O. R., Gao, R. S., Tarasick, D., Leblanc, T., and Sweeney, C.: Long-term ozone trends at rural ozone monitoring sites across the United States, 1990-2010, J. Geophys. Res., 117, D22307, doi:10.1029/2012jd018261, 2012.

Daumont, D., Brion, J., Charbonnier, J., and Malicet, J.: Ozone UV Spectroscopy I: Absorption Cross-Sections at Room Temperature, J. Atmos Chem., 15, 145-155, 10.1007/bf00053756, 1992

25 De Mazière, M., Thompson, A. M., Kurylo, M. J., Wild, J. D., Bernhard, G., Blumenstock, T., Braathen, G. O., Hannigan, J. W., Lambert, J. C., Leblanc, T., McGee, T. J., Nedoluha, G., Petropavlovskikh, I., Seckmeyer, G., Simon, P. C., Steinbrecht, W., and Strahan, S. E.: The Network for the Detection of Atmospheric Composition Change (NDACC): history, status and perspectives, Atmos. Chem. Phys., 18, 4935-4964, doi:10.5194/acp-18-4935-2018, 2018.

De Young, R., Carrion, W., Ganoe, R., Pliutau, D., Gronoff, G., Berkoff, T., and Kuang, S.: Langley mobile ozone lidar:

30 ozone and aerosol atmospheric profiling for air quality research, Appl. Optics, 56, 721-730, doi:10.1364/ao.56.000721, 2017.

Farris, B., Gronoff, G., Carrion, W., Knepp, T., Pippin, M., and Berkoff, T.: Demonstration of an off-axis parabolic receiver for near-range retrieval of lidar ozone profiles, Atmos. Meas. Tech., Submitted, 2018.

Granados-Muñoz, M. J., and Leblanc, T.: Tropospheric ozone seasonal and long-term variability as seen by lidar and surface measurements at the JPL-Table Mountain Facility, California, Atmos. Chem. Phys., 16, 9299-9319, doi:10.5194/acp-16-9299-2016, 2016.

Gronoff, G., Robinson, J., Berkoff, T., Swap, R., Farris, B., Schroeder, J., Halliday, H., Knepp, T., Spinei, H., Carrion, W., Adcock, E., Johns, Z., Allen, D., and Pippin, M.: A Method for Observing Near Range Point Source Induced O 3 Titration Events Using Co-located Lidar and Pandora measurements, Atmos. Meas. Tech., Submitted, 2018.

IPCC: Summary for Policymakers, in: Climate Change 2013: The Physical Science Basis. Contribution of Working Group I to the Fifth Assessment Report of the Intergovernmental Panel on Climate Change, edited by: Stocker, T. F., Qin, D., Plattner, G.-K., Tignor, M., Allen, S. K., Boschung, J., Nauels, A., Xia, Y., Bex, V., and Midgley, P. M., Cambridge University Press, Cambridge, UK and New York, NY, USA, 2013

Johnson, M. S., Liu, X., Zoogman, P., Sullivan, J., Newchurch, M. J., Kuang, S., Leblanc, T., and McGee, T.: Evaluation of potential sources of a priori ozone profiles for TEMPO tropospheric ozone retrievals, Atmos. Meas. Tech., 11, 3457-3477, doi:10.5194/amt-11-3457-2018, 2018.

Kempfer, U., Carnuth, W., Lotz, R., and Trickl, T.: A wide-range ultraviolet lidar system for tropospheric ozone measurements: Development and application, Rev. Sci. Instr., 65, 3145-3164, 10.1063/1.1144769, 1994.

Komhyr, W. D.: Electrochemical concentration cells for gas analysis, Ann. Geophys., 25, 203-210, 1969.

Kuang, S., Newchurch, M. J., Burris, J., and Liu, X.: Ground-based lidar for atmospheric boundary layer ozone measurements, Appl. Opt., 52, 3557-3566, doi:10.1364/ao.52.003557, 2013.

Langford, A. O., Brioude, J., Cooper, O. R., Senff, C. J., Alvarez, R. J., Hardesty, R. M., Johnson, B. J., and Oltmans, S. J.: Stratospheric influence on surface ozone in the Los Angeles area during late spring and early summer of 2010, J. Geophys. Res., 117, D00V06, doi:10.1029/2011JD016766, 2012

Langford, A. O., Senff, C. J., Alvarez Ii, R. J., Brioude, J., Cooper, O. R., Holloway, J. S., Lin, M. Y., Marchbanks, R. D., Pierce, R. B., Sandberg, S. P., Weickmann, A. M., and Williams, E. J.: An overview of the 2013 Las Vegas Ozone Study (LVOS): Impact of stratospheric intrusions and long-range transport on surface air quality, Atmos. Environ., 109, 305-322, doi:10.1016/j.atmosenv.2014.08.040, 2015.

Langford, A. O., Alvarez II, R. J., Kirgis, G., Senff, C., Caputi, J. D., Conley, S. A., Faloona, I. C., Iraci, L. T., Marrero, J. E., McNamara, M. E., Ryoo, J.-M., and Yates, E. L.: Lidar and aircraft profiling of ozone above the central 1 San Joaquin Valley during the California Baseline Ozone Transport Study (CABOTS), J. Geophys. Res., Submitted, 2018.

Leblanc, T., Walsh, T. D., McDermid, I. S., Toon, G. C., Blavier, J. F., Haines, B., Read, W. G., Herman, B., Fetzer, E., Sander, S., Pongetti, T., Whiteman, D. N., McGee, T. G., Twigg, L., Sumnicht, G., Venable, D., Calhoun, M., Dirisu, A., Hurst, D., Jordan, A., Hall, E., Miloshevich, L., Vomel, H., Straub, C., Kampfer, N., Nedoluha, G. E., Gomez, R. M., Holub, K., Gutman, S., Braun, J., Vanhove, T., Stiller, G., and Hauchecorne, A.: Measurements of Humidity in the Atmosphere and

Validation Experiments (MOHAVE)-2009: overview of campaign operations and results, Atmos. Meas. Tech., 4, 2579-2605, doi:10.5194/amt-4-2579-2011, 2011.

Leblanc, T., McDermid, I. S., and Walsh, T. D.: Ground-based water vapor raman lidar measurements up to the upper troposphere and lower stratosphere for long-term monitoring, Atmos. Meas. Tech., 5, 17-36, 10.5194/amt-5-17-2012, 2012.

5   Leblanc, T., Sica R., van Gijsel, J. A. E., Godin-Beekmann, S., Haefele, A., Trickl, T., Payen, G., and Liberti, G.: Standardized definition and reporting of vertical resolution and uncertainty in the NDACC lidar ozone and temperature algorithms, ISSI Team on NDACC Lidar Algorithms Report, available for download at http://www.issibern.ch/teams/ndacc/ISSI_Team_Report.htm, 2015.

Leblanc, T., Sica, R. J., van Gijsel, J. A. E., Godin-Beekmann, S., Haefele, A., Trickl, T., Payen, G., and Gabarrot, F.: 10   Proposed standardized definitions for vertical resolution and uncertainty in the NDACC lidar ozone and temperature algorithms – Part 1: Vertical resolution, Atmos. Meas. Tech., 9, 4029-4049, doi:10.5194/amt-9-4029-2016, 2016a.

Leblanc, T., Sica, R. J., van Gijsel, J. A. E., Godin-Beekmann, S., Haefele, A., Trickl, T., Payen, G., and Liberti, G.: Proposed standardized definitions for vertical resolution and uncertainty in the NDACC lidar ozone and temperature algorithms – Part 2: Ozone DIAL uncertainty budget, Atmos. Meas. Tech., 9, 4051-4078, doi:10.5194/amt-9-4051-2016, 15   2016b.

Malicet, J., Daumont, D., Charbonnier, J., Parisse, C., Chakir, A., and Brion, J.: Ozone uv spectroscopy .2. Absorption cross-sections and temperature-dependence, J. Atmos Chem., 21, 263-273, 10.1007/bf00696758, 1995

McDermid, I. S., Godin, S. M., and Walsh, T. D.: Results from the Jet-Propulsion-Laboratory stratospheric ozone lidar during STOIC 1989, J. Geophys. Res., 100, 9263-9272, doi:10.1029/94jd02148, 1995.

20   McDermid, I. S., Beyerle, G., Haner, D. A., and Leblanc, T.: Redesign and improved performance of the tropospheric ozone lidar at the Jet Propulsion Laboratory Table Mountain Facility, Appl. Opt., 41, 7550-7555, 2002.

Mégie, G., Allain, J. Y., Chanin, M. L., and Blamont, J. E.: Vertical Profile of Stratospheric Ozone by Lidar Sounding from Ground, Nature, 270, 329-331, 1977.

Nakazato, M., Nagai, T., Sakai, T., and Hirose, Y.: Tropospheric ozone differential-absorption lidar using stimulated Raman 25   scattering in carbon dioxide, Appl. Optics, 46, 2269-2279, doi:10.1364/ao.46.002269, 2007.

Newsom, R. K., Turner, D. D., Mielke, B., Clayton, M., Ferrare, R., and Sivaraman, C.: Simultaneous analog and photon counting detection for Raman lidar, Appl. Opt., 48, 3903–3914, 2009

Savitzky, A., and Golay, M. J. E.: Smoothing and differentiation of data by simplified least squares procedures, Anal. Chem., 36, 1627-1639, 1964.

30   Senff, C. J., Alvarez, R. J., Hardesty, R. M., Banta, R. M., and Langford, A. O.: Airborne lidar measurements of ozone flux downwind of Houston and Dallas, J. Geophys. Res., 115, doi:10.1029/2009jd013689, 2010.

Smit, H. G. J., Straeter, W., Johnson, B. J., Oltmans, S. J., Davies, J., Tarasick, D. W., Hoegger, B., Stubi, R., Schmidlin, F. J., Northam, T., Thompson, A. M., Witte, J. C., Boyd, I., and Posny, F.: Assessment of the performance of ECC-

ozonesondes under quasi-flight conditions in the environmental simulation chamber: Insights from the Juelich Ozone Sonde Intercomparison Experiment (JOSIE), J. Geophys. Res., 112, D19306, doi:10.1029/2006jd007308, 2007.

Strawbridge, K. B., Developing a portable, autonomous aerosol backscatter lidar for network 13 or remote operations, Atmos. Meas. Tech., 6, 801-816, doi:10.5194/amt-6-801-14-2013, 2013.

5 Strawbridge, K. B., Travis, M. S., Firanski, B. J., Brook, J. R., Staebler, R., and Leblanc T., A fully autonomous ozone, aerosol, and night time water vapor LIDAR: a synergistic approach to profiling the atmosphere in the Canadian oil sands region, Atmos. Meas. Tech. Discuss., doi:10.5194/amt-2018-108, 2018.

Sullivan, J. T., McGee, T. J., Sumnicht, G. K., Twigg, L. W., and Hoff, R. M.: A mobile differential absorption lidar to measure sub-hourly fluctuation of tropospheric ozone profiles in the Baltimore–Washington, D.C. region, Atmos. Meas.
10 Tech., 7, 3529-3548, doi:10.5194/amt-7-3529-2014, 2014.

Sullivan, J. T., McGee, T. J., Leblanc, T., Sumnicht, G. K., and Twigg, L. W.: Optimization of the GSFC TROPOZ DIAL retrieval using synthetic lidar returns and ozonesondes - Part 1: Algorithm validation, Atmos. Meas. Tech., 8, 4133-4143, 10.5194/amt-8-4133-2015, 2015.

Sullivan, J. T., McGee, T. J., Langford, A. O., Alvarez, R. J., Senff, C. J., Reddy, P. J., Thompson, A. M., Twigg, L. W.,
15 Sumnicht, G. K., Lee, P., Weinheimer, A., Knote, C., Long, R. W., and Hoff, R. M.: Quantifying the contribution of thermally driven recirculation to a high-ozone event along the Colorado Front Range using lidar, Journal of Geophysical Research: Atmospheres, 121, 10,377-310,390, doi:10.1002/2016JD025229, 2016.

Wang, L. H., Newchurch, M. J., Alvarez, R. J., Berkoff, T. A., Brown, S. S., Carrion, W., De Young, R. J., Johnson, B. J., Ganoe, R., Gronoff, G., Kirgis, G., Kuang, S., Langford, A. O., Leblanc, T., McDuffie, E. E., McGee, T. J., Pliutau, D.,
20 Senff, C. J., Sullivan, J. T., Sumnicht, G., Twigg, L. W., and Weinheimer, A. J.: Quantifying TOLNet ozone lidar accuracy during the 2014 DISCOVER-AQ and FRAPPE campaigns, Atmospheric Measurement Techniques, 10, 3865-3876, doi:10.5194/amt-10-3865-2017, 2017.

Weber, M., Gorshelev, V., and Serdyuchenko, A.: Uncertainty budgets of major ozone absorption cross sections used in UV remote sensing applications, Atmos. Meas. Tech., 9, 4459-4470, 10.5194/amt-9-4459-2016, 2016.

25 World Health Organization: Health aspects of air pollution with particulate matter, ozone and nitrogen dioxide: report on a WHO working group, 13–15 January 2003, Bonn, Germany, 2003

World Meteorological Organization: Quality Assurance and Quality Control for Ozonesonde Measurements in GAW, October 2014, Geneva, Switzerland, 2014

Zhang, Y., Yi, F., Kong, W., and Yi, Y.: Slope characterization in combining analog and photon count data from
30 atmospheric lidar measurements, Appl. Opt., 53, 7312–7320, 2014

Zoogman, P., Jacob, D. J., Chance, K., Liu, X., Lin, M., Fiore, A., and Travis, K.: Monitoring high-ozone events in the US Intermountain West using TEMPO geostationary satellite observations, Atmos. Chem. Phys., 14, 6261-6271, doi:10.5194/acp-14-6261-2014, 2014.

Tables

Table 1: Transmitter Configuration of the TOLNet Ozone Lidar Instruments Used During SCOOP

	AMOLITE	LMOL	TMTOL	TOPAZ	TROPOZ
Laser type	Nd:YAG Quadrupled	Ce:LiCAF Tunable	Nd:YAG Quadrupled	Ce:LiCAF Tunable	Nd:YAG Quadrupled
Laser wavelength (nm)	266.0	280-298	266.0	285-310	266.0
Laser rep. rate (Hz)	20	1000/2	30	1000/3	50
Power ON/OFF (W)	0.9	0.075	1.1	0.03	0.8
Pulse Energy (mJ)	45	0.15	40	0.05	15
Raman cell	CO_2 second and third Stokes	N/A	H_2 first Stokes D_2 first Stokes	N/A	H_2 first Stokes D_2 first Stokes
DIAL wavelengths during SCOOP (nm)	ON: 287.2 OFF: 299.1	ON: 287.1 OFF: 292.7	ON: 288.9 OFF: 299.1	ON: 286-287 OFF: 293-294	ON: 288.9 OFF: 299.1
Direction of Emission	Fixed Zenith	Fixed Zenith	Fixed Zenith	Scanning 2º - Zenith	Fixed Zenith

Table 2: Receiver Configuration of the TOLNet Ozone Lidar Instruments Used During SCOOP

	AMOLITE	LMOL	TMTOL	TOPAZ	TROPOZ
Telescope size	1 x 35 cm	1 x 40 cm	1 x 91 cm 2 x 5 cm	1 x 50 cm	1 x 45 cm 4 x 2.5 cm
Spectral Separation	2 x IF	1 x SWP	2 x SWP 4 x IF	N/A	6 x IF
Detectors	2 x PMT R7400U-03	1 x PMT R7400-U03	4 x PMT H5783P-06	2 x PMT HP9880-110	6 x PMT HP9880-110
Data Recorders	2 x Licel TR ADC 12 bits PC 250 MHz	1 x Licel TR ADC 12 bits PC 250 MHz	4 x Licel TR ADC 16 bits PC 250 MHz	2 x Licel TR ADC 16 bits PC 250 MHz	6 x Licel TR ADC 12 bits PC 250 MHz

ADC = Analog-to-Digital Converter; PC = Photon-counting; PMT = Photomultiplier; TR = Transient Recorder

Table 3: Data Acquisition Configuration of the TOLNet Ozone Lidar Instruments Used During SCOOP

	AMOLITE	LMOL	TMTOL	TOPAZ	TROPOZ
Data Acquisition Software	Custom 2 ADC channels 2 PC channels	Licel 2 ADC channels 2 PC channels	Custom 4 ADC channels 4 PC channels	Licel 2 ADC channels 2 PC channels	Licel 6 ADC channels 6 PC channels
Range Sampling	3.75 m	7.5 m	3.75 m	7.5 m	15 m
Temporal Sampling	1 min	20 s	5 min	1 s	20 s
Instrument Elevation	2270 m	2270 m	2285 m	2285 m	2285 m
Distance from TMF ozonesonde launch location	300 m	300 m	10 m	10 m	15 m

Table 4: Lidar Data Availability During SCOOP

Date (Local Time)	Date UT [1]	AMOLITE (UT) [2]	LMOL (UT) [2]	TMTOL (UT) [2]	TOPAZ (UT) [2]	TROPOZ (UT) [2]
August 9	2016/08/09	07:00-23:59	/	/	/	/
	2016/08/10	00:00-06:59	03:30-05:55	03:44-05:45	/	03:40-06:17
August 10	2016/08/10	07:00-23:59	18:45-22:15	/	/	/
	2016/08/11	00:00-06:59	00:00-05:15	02:24-04:24	04:44-05:24	02:33-04:28
August 11	2016/08/11	07:00-23:59	18:30-21:45	19:03-21:39	19:19-23:59	19:57-21:39
	2016/08/12	00:00-06:59	00:00-01:35	00:04-04:21	00:00-02:39	00:00-03:15
August 12	2016/08/12	07:00-18:08	11:10-18:40	11:00-19:15	10:55-19:15	11:07-19:09
	2016/08/13	01:24-06:59	/	/	/	/
August 13	2016/08/13	07:00-23:59	18:45-23:59	17:58-23:59	18:18-23:59	18:57-23:59
	2016/08/14	00:00-06:59	00:00-05:00	00:01-02:41	00:00-05:08	00:00-05:47
August 14	2016/08/14	07:00-23:59	/	/	/	/
	2016/08/15	00:00-06:59				
August 15	2016/08/15	07:00-23:59	11:00-23:59	10:36-23:59	10:15-23:59	10:59-23:59
	2016/08/16	00:00-06:59	00:00-06:00	00:27-06:42	00:00-05:35	00:00-05:13
August 16	2016/08/16	07:00-23:59	19:30-21:55	20:49-22:41	19:28-22:48	21:03-22:40
	2016/08/17	00:00-06:59	/	/	/	/
Total	7 days	200+ hours	52 hours	49 hours	48 hours	47 hours

[1] Change of UT date occurs at 17:00 Local Time (PDT); [2] Start and end times

Table 5: Ozonesonde and 30-min Lidar Coincidences used to obtained the SCOOP Level 2 data

Ozonesonde Date/Time UT	Ozonesonde name	AMOLITE (UT)	LMOL (UT)	TMTOL (UT)	TOPAZ (UT)	TROPOZ (UT)
2016/08/10 04:01	tm073	04:01-04:31	/	04:05-04:35	/	04:01-04:32
2016/08/11 03:01	tm075	03:01-03:31	03:00-03:30	03:04-03:34	04:40-05:10	03:01-03:32
2016/08/11 20:01	tm076	/	20:00-20:30	20:00-20:27	20:01-20:31	20:01-20:31
2016/08/12 02:01	tm077	02:01-02:31	01:30-02:00	02:00-02:34	02:01-02:31	02:01-02:32
2016/08/12 11:32	tm078	11:32-12:02	11:30-12:00	11:34-12:04	11:21-11:47	11:31-12:02
2016/08/12 14:39	tm079	14:39-15:09	14:39-15:09	14:39-15:08	14:13-14:43	14:39-15:09
2016/08/12 17:33	tm080	/	17:38-18:08	17:35-18:05	17:33-18:03	17:33-18:04
2016/08/13 19:01	tm081	/	19:00-19:30	19:03-19:32	19:01-19:31	19:01-19:31
2016/08/14 00:44	tm082	00:44-01:14	00:40-01:10	00:47-01:17	00:44-01:14	00:43-01:14
2016/08/14 04:15	tm083	04:15-04:45	04:15-04:45	/	04:15-04:45	04:15-04:45
2016/08/15 11:37	tm084	11:37-12:07	11:35-12:05	11:37-12:09	11:37-12:07	11:36-12:07
2016/08/15 15:32	tm085	15:32-16:02	15:30-16:00	15:33-16:03	15:32-16:02	15:31-16:02
2016/08/15 17:42	tm086	17:42-18:12	17:40-18:10	17:45-18:15	17:42-18:12	17:41-18:10
2016/08/15 21:47	tm087	21:53-22:23	21:45-22:15	21:50-22:20	21:47-22:17	21:46-22:17
2016/08/16 01:02	tm088	01:02-01:32	01:00-01:30	01:03-01:33	01:02-01:32	01:01-01:32
2016/08/16 03:59	tm089	03:59-04:29	03:59-04:29	04:05-04:34	03:59-04:29	03:58-04:28
2016/08/16 21:03	tm090	21:03-21:33	21:00-21:30	21:03-21:33	21:03-21:33	21:21-21:52

Table 6: Summary of mean biases found during SCOOP between a single instrument and all the other ones, and summary of key statistics characterizing the lidar instruments' capability

All altitudes: a.s.l. Ground is at 2.3 km	All Lidars w.r.t. ECC	AMOLITE w.r.t. all others	LMOL w.r.t. all others	TMTOL w.r.t. all others	TOPAZ w.r.t. all others	TROPOZ w.r.t. all others
Mean bias [6] 3-10 km	1.7% 0.7 ppbv	1.9% 0.2 ppbv	1.5% 0.3 ppbv	-1.2% -0.1 ppbv	1.3% 0.5 ppbv	-1.6% -0.4 ppbv
R.M.S. [6] 3-10 km	2.4% 1.6 ppbv	4.4% 2.2 ppbv	3.1% 1.6 ppbv	5.1% 3.4 ppbv	3.1% 1.8 ppbv	3.5% 1.9 ppbv
Effect. Vert. Resol. 3-5 km	/	300-m	150-m	600-m [2]	500 m [1]	500 m [1]
Precison (30-min) 3-5 km	/	1.5 ppbv	1 ppbv	5 ppbv [2]	Not available	1.5 ppbv
Effect. Vert. Resol. 5-8 km	/	700-m	600-m	900-m [2]	1000 m [1]	1000 m [1]
Precison (30-min) 5-8 km	/	Night: 2.5 ppbv Day: 1.5 ppbv	1 ppbv	Night: 9 ppbv [2] Day: 4 ppbv [3]	Not available	1.5 ppbv
Effect. Vert. Resol. 8-11 km	/	1400-m	2000-m	1000-m [3]	1500 m [1]	1500 m [1]
Precison (30-min) 8-11 km	/	Night: 5 ppbv Day: 1.5 ppbv	Night: 1 ppbv Day: 2 ppbv	Night: 5 ppbv [3] Day: 9 ppbv [3]	Not available	Night: 3 ppbv Day: 7 ppbv
Systematic Uncert. 3-8 km	/	2 ppbv	4 ppbv	2 ppbv	Not available	4 ppbv
Systematic Uncert. 8-11 km	/	Night: 2 ppbv Day: 4 ppbv [5]	Night: 4 ppbv Day: 10 ppbv [5]	Night: 3 ppbv [4] Day: 2 ppbv	Not available	Night: 4 ppbv Day: 5 ppbv [5]

[1] Use of SCOOP effective vertical resolution scheme

[2] Use of TMTOL low-intensity range

[3] Use of TMTOL high-intensity range

[4] Use of TMTOL hybrid-channel for lower stratospheric measurements

[5] Increased background noise due to bright conditions

[6] Because of the strong sampling heterogeneity, a linear relation between ppbv and % should not be expected

Figures
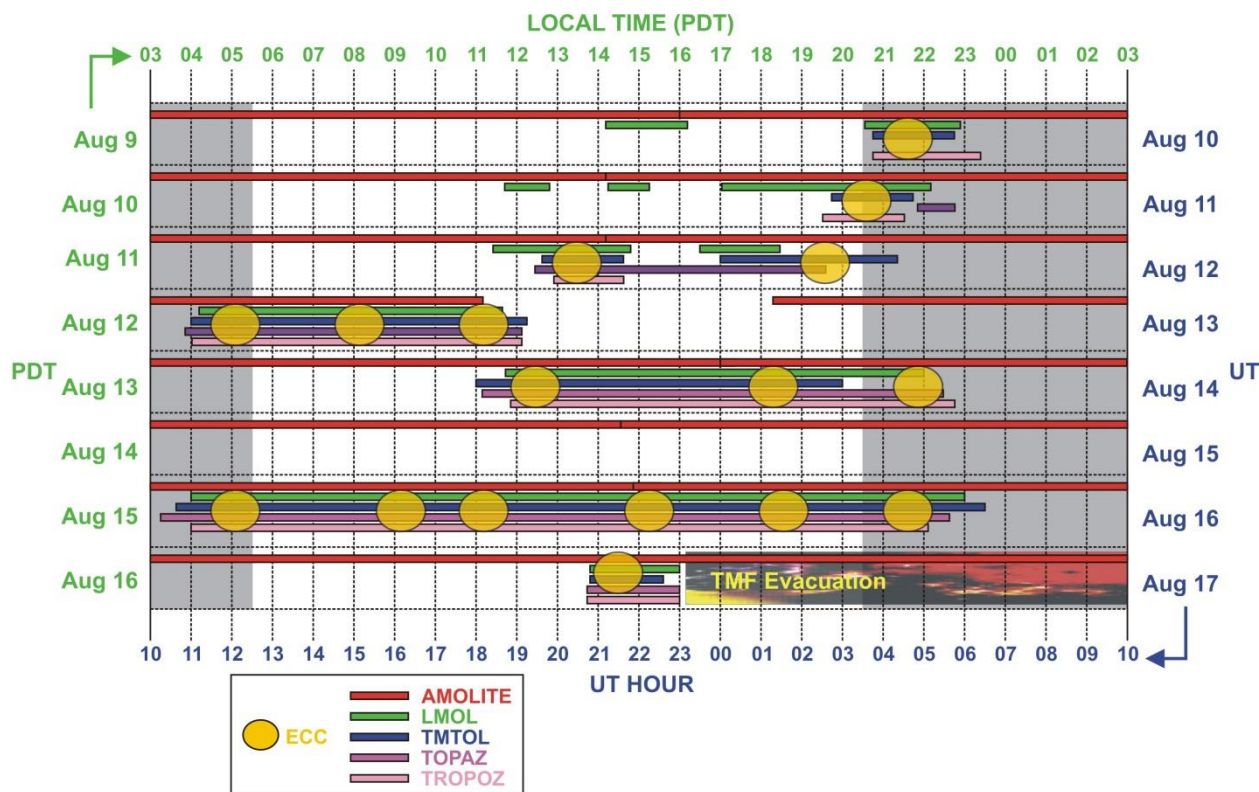
Figure 1: SCOOP Campaign operation schedule for the five participating TOLNet lidars and 17 ECC ozonesonde launches. Grey-shaded areas denote night time.
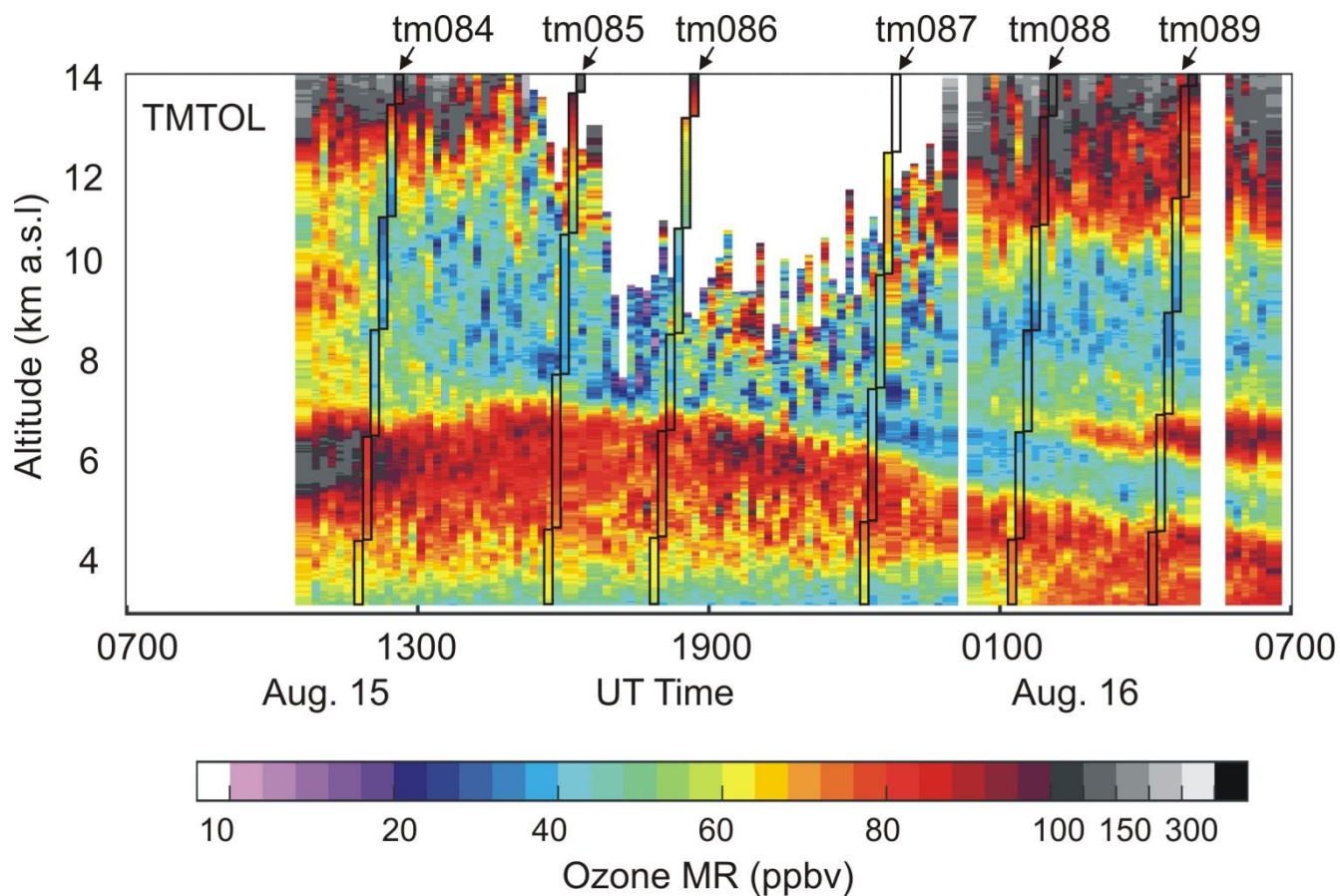
Figure 2: Ozone time-altitude cross-section obtained by the JPL TMTOL lidar on August 14, 2016 (time resolution: 10 minutes). Ozone measured by the six ozonesondes launched on that day is superimposed using thin, coloured, slanted rectangles.
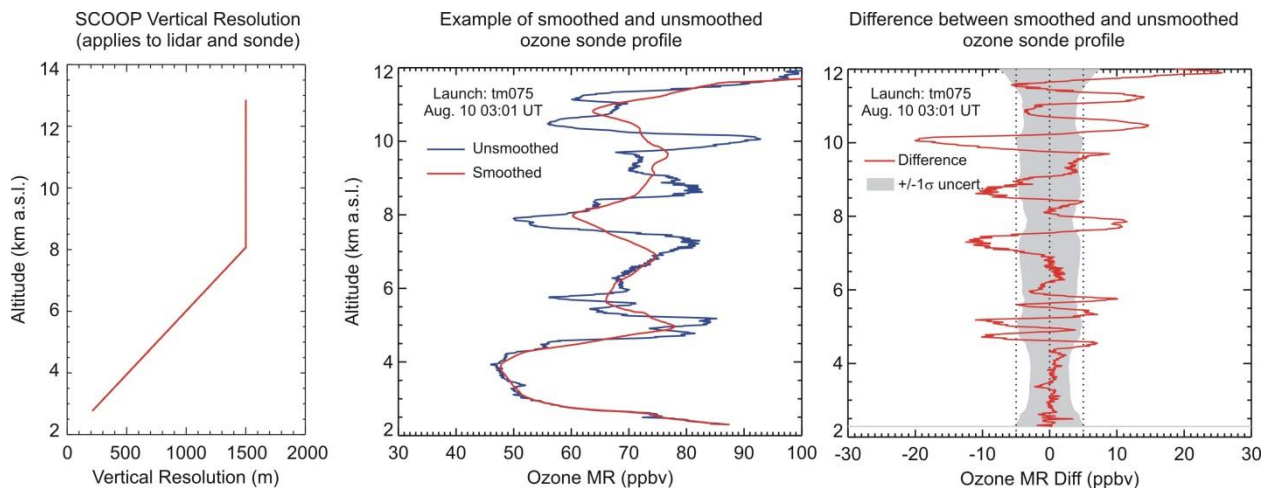
Figure 3: Left panel: Effective vertical resolution scheme used for all lidars and ozonesonde profiles for the blind validation phase of SCOOP (referred to as "SCOOP level 2" data, see text for details). Middle panel: Example of ozonesonde profile before (blue) and after (red) the SCOOP vertical resolution scheme is applied. Right panel: Difference between smooth and unsmoothed ozonesonde profiles shown in middle panel. Grey shaded area points out +/- one standard uncertainty.
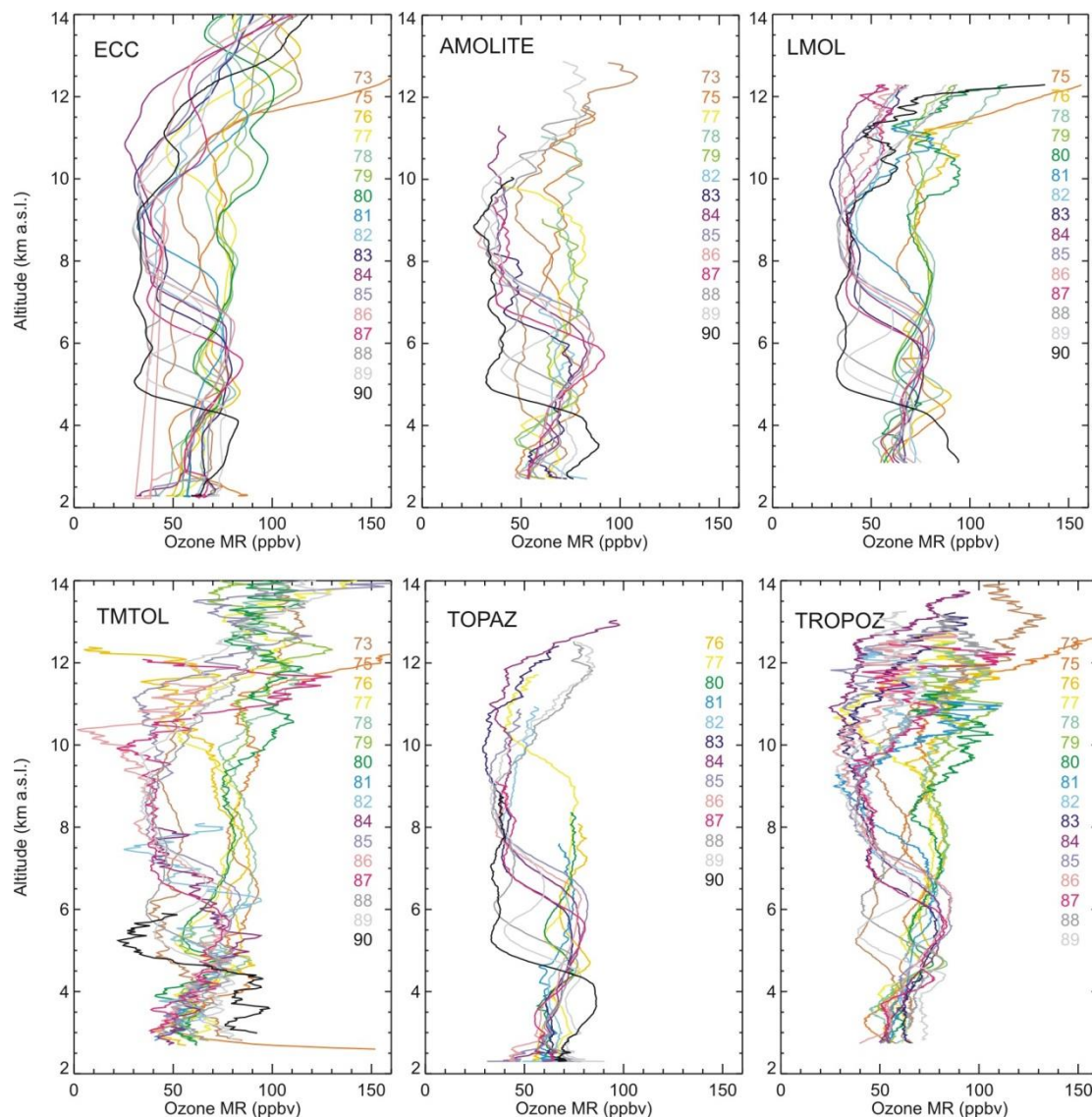
Figure 4: Top-left panel: ECC ozonesonde profiles measured during each of the 17 launches performed during the SCOOP campaign (launch numbers listed on the side). All other panels: Ozone profiles measured by lidar during each available coincident sonde-lidar measurements. Coincidences (number and list) vary by instrument.
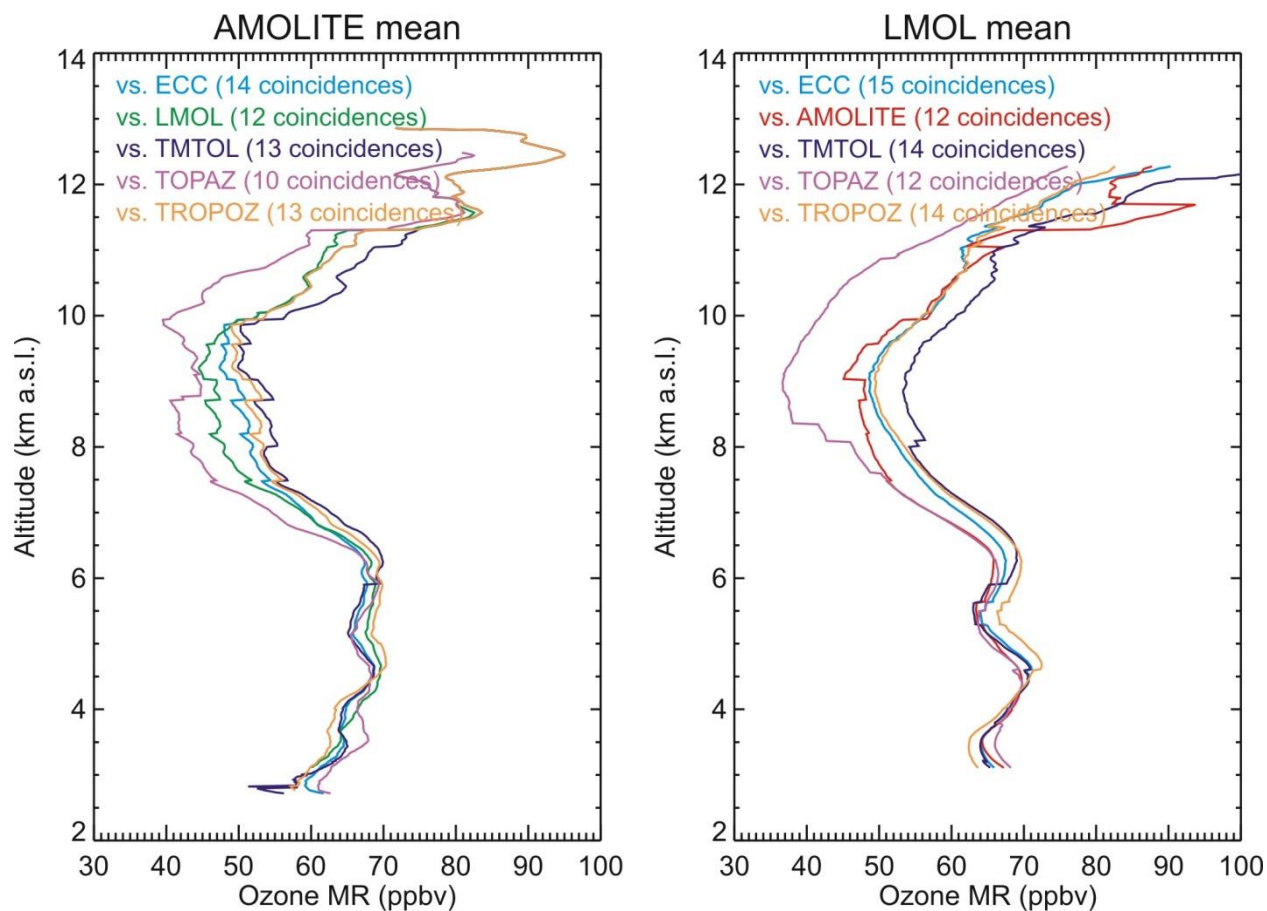
Figure 5: Mean AMOLITE (left panel) and LMOL (right panel) ozone profiles computed using one-on-one coincidences with each of the other instruments.
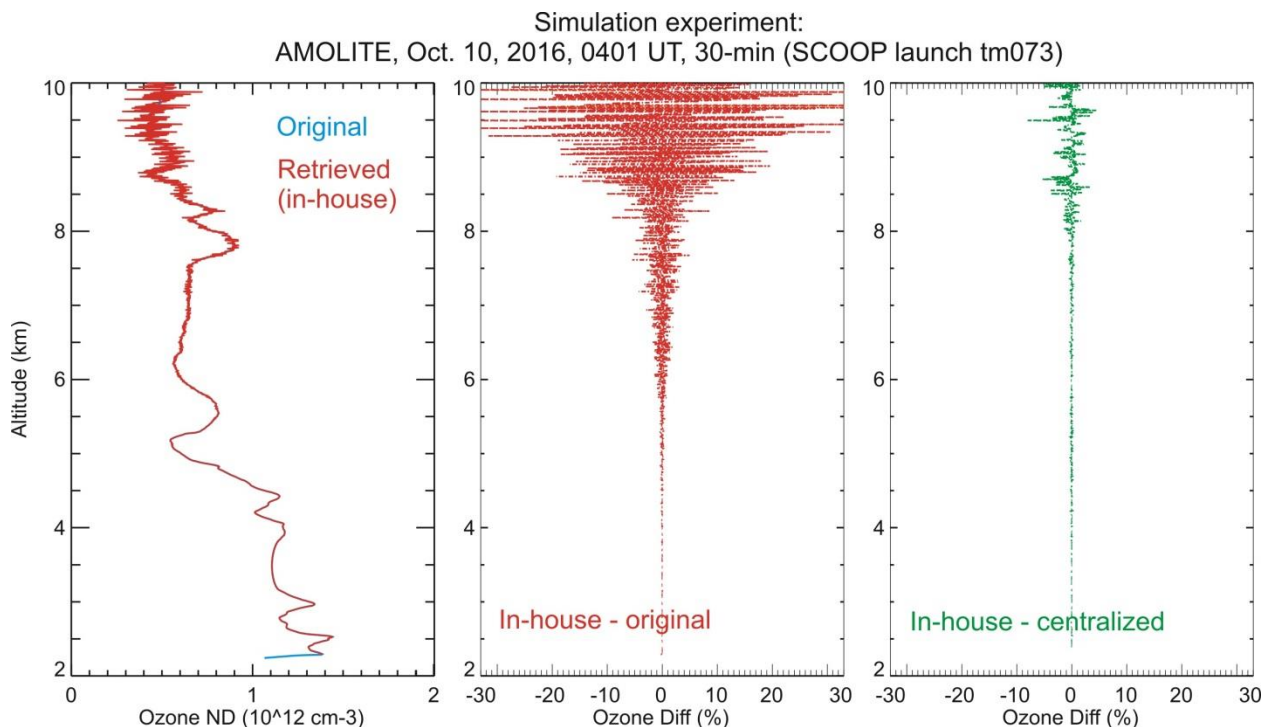
Figure 6: Example of algorithm validation result (see text for details). Left panel: Ozone profile used in the algorithm validation forward model (cyan curve), and ozone profile retrieved by the AMOLITE in-house data processing (red curve) using the simulated lidar signals produced by the forward model. Middle panel: Difference (%) between the retrieved and original ozone profiles shown in left panel. Right panel: Difference between the AMOLITE-retrieved and GLASS-retrieved profiles (see text for details).
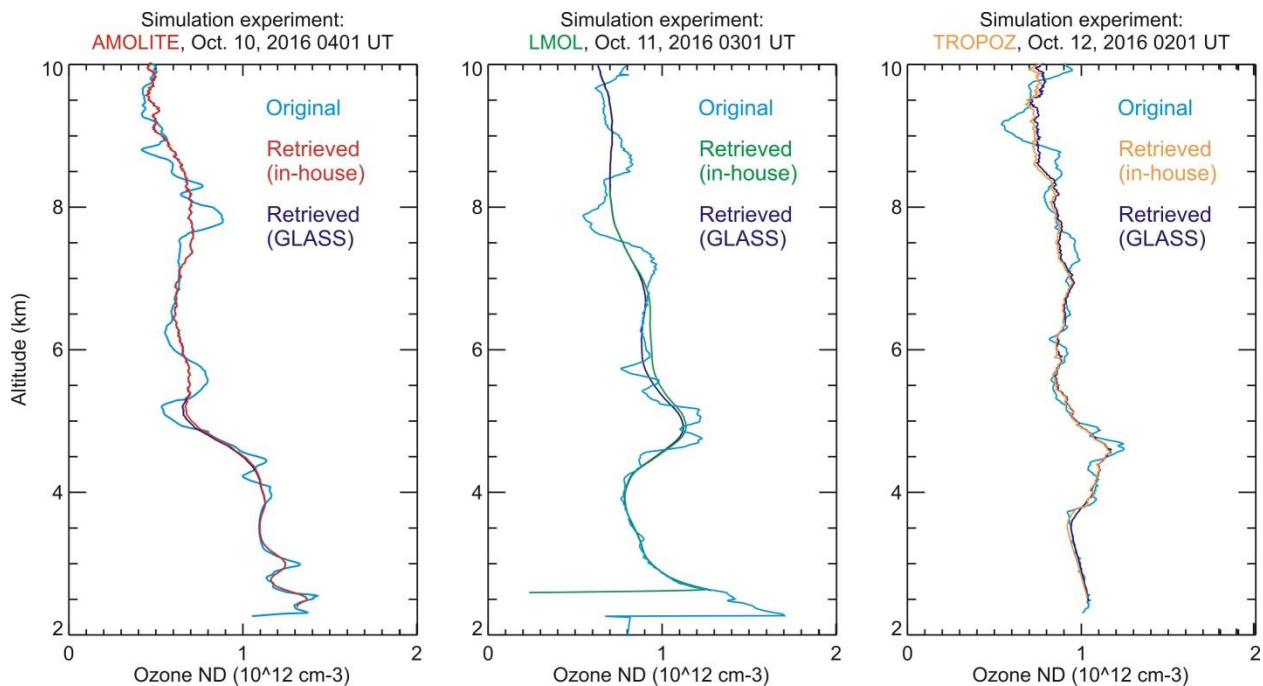
Figure 7: Another example of algorithm validation result, this time testing vertical resolution (see text for details). Left panel: Ozone profile used in the forward model (cyan curve), and ozone profile retrieved by the AMOLITE in-house data processing (red curve) and GLASS (blue curve), both at the same, prescribed SCOOP vertical resolution. Middle and right panels: Same as left panel, but for LMOL and TROPOZ respectively.
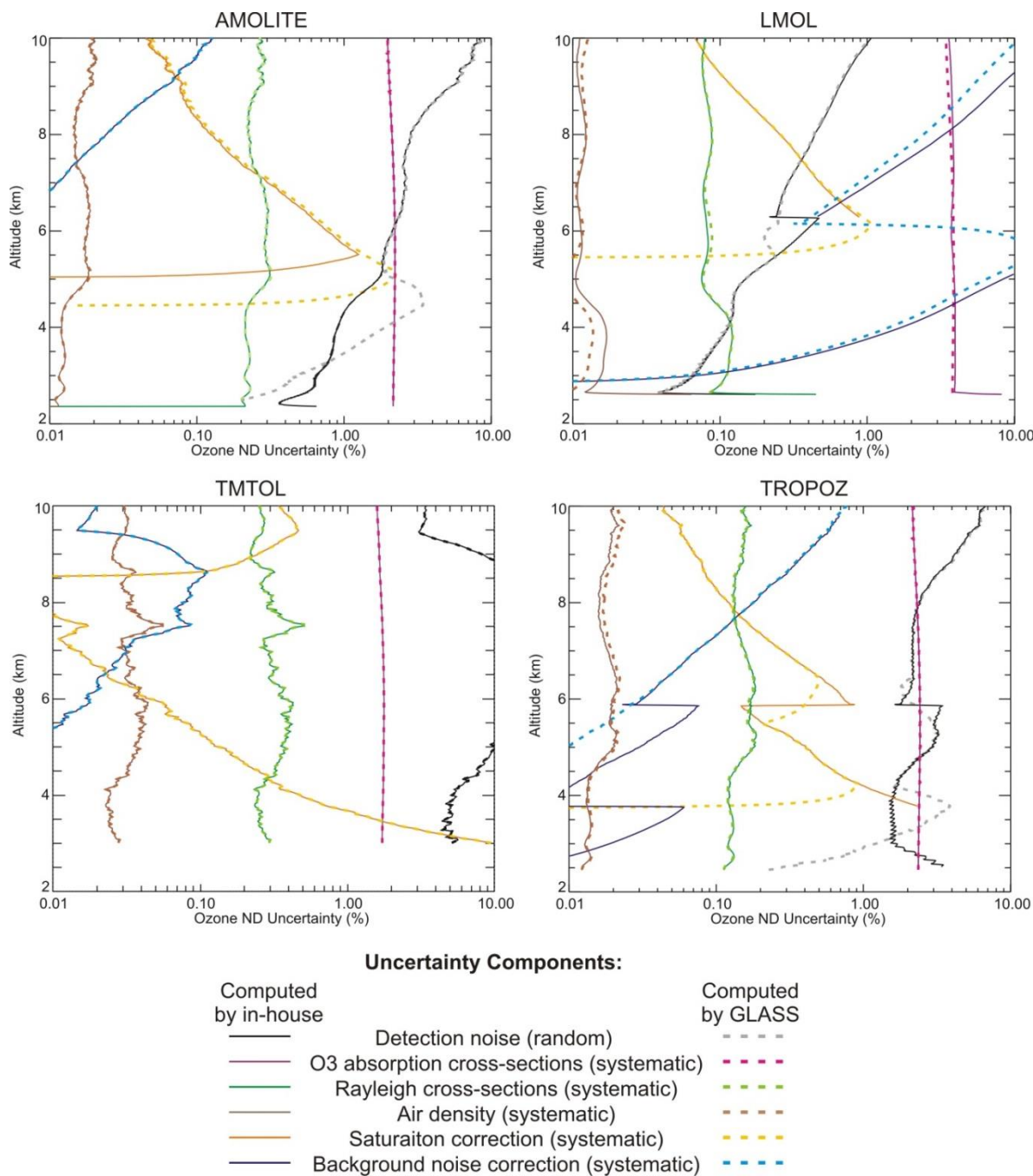
Figure 8: NDACC-standardized ozone uncertainty budget for four of the five TOLNet lidars participating to SCOOP, including one random component (black: detection noise), and 5 systematic components (pink: ozone absorption cross-sections, green: Rayleigh cross-sections, blue: background noise correction, brown: air density, yellow: saturation correction). Solid curves denote ozone uncertainty (%) computed by the in-house data processing algorithms while dash curves denote the ozone uncertainty computed by the GLASS (reference transfer).
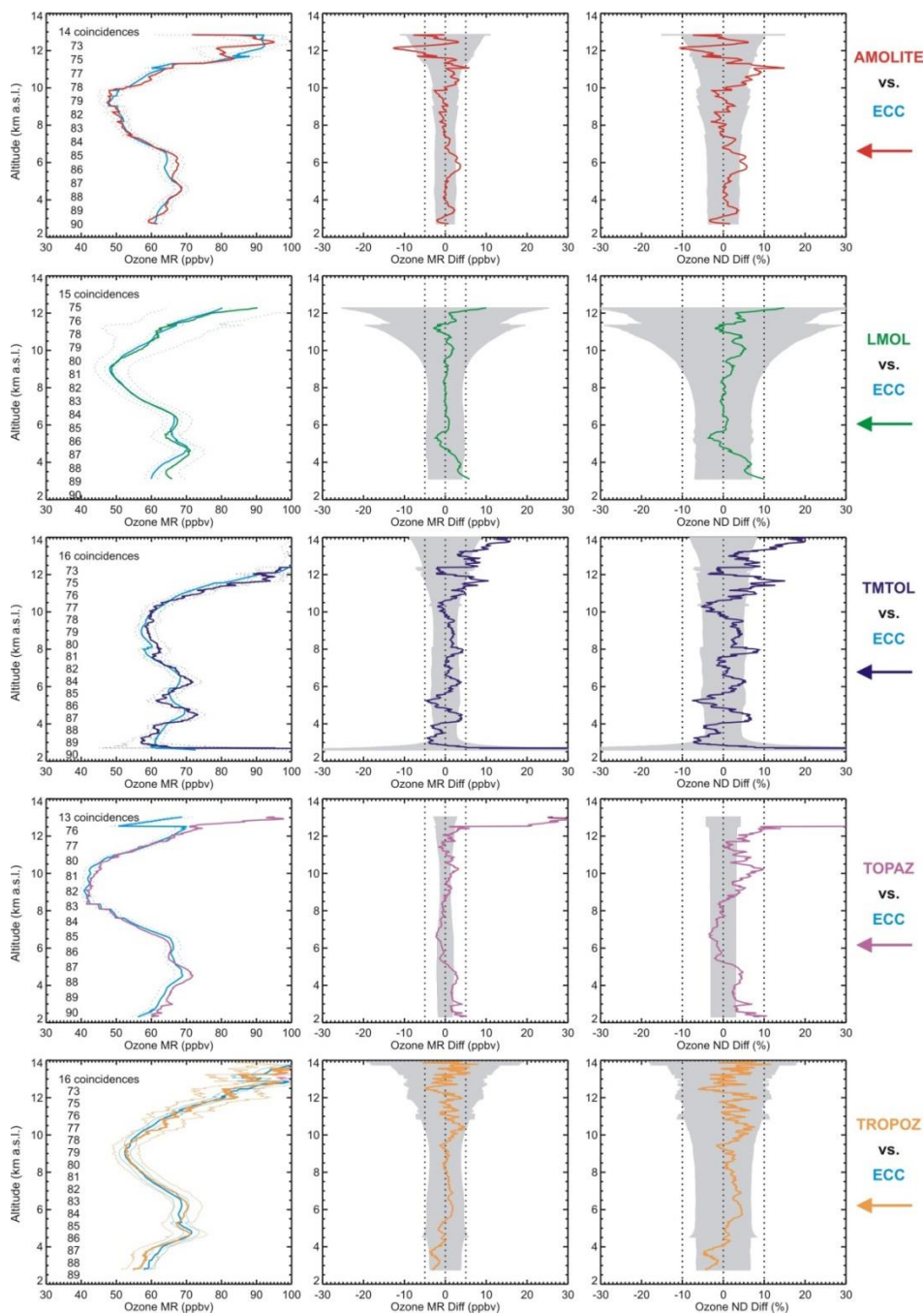
Figure 9: One-on-one ozone profile intercomparison between ECC ozonesonde (cyan curves) and lidar (from top to bottom: AMOLITE in red, LMOL in green, TMTOL in blue, TOPAZ in purple, and TROPOZ in yellow). In the left panels, the thin dotted lines represent the ozone profiles +/- uncertainty. Each coincidence is identified by the ozonesonde launch number. The middle and right panels show the differences between lidar and ozonesonde in ppbv and % respectively (ozonesonde is the reference). The grey-shaded areas denote the combined total uncertainty.
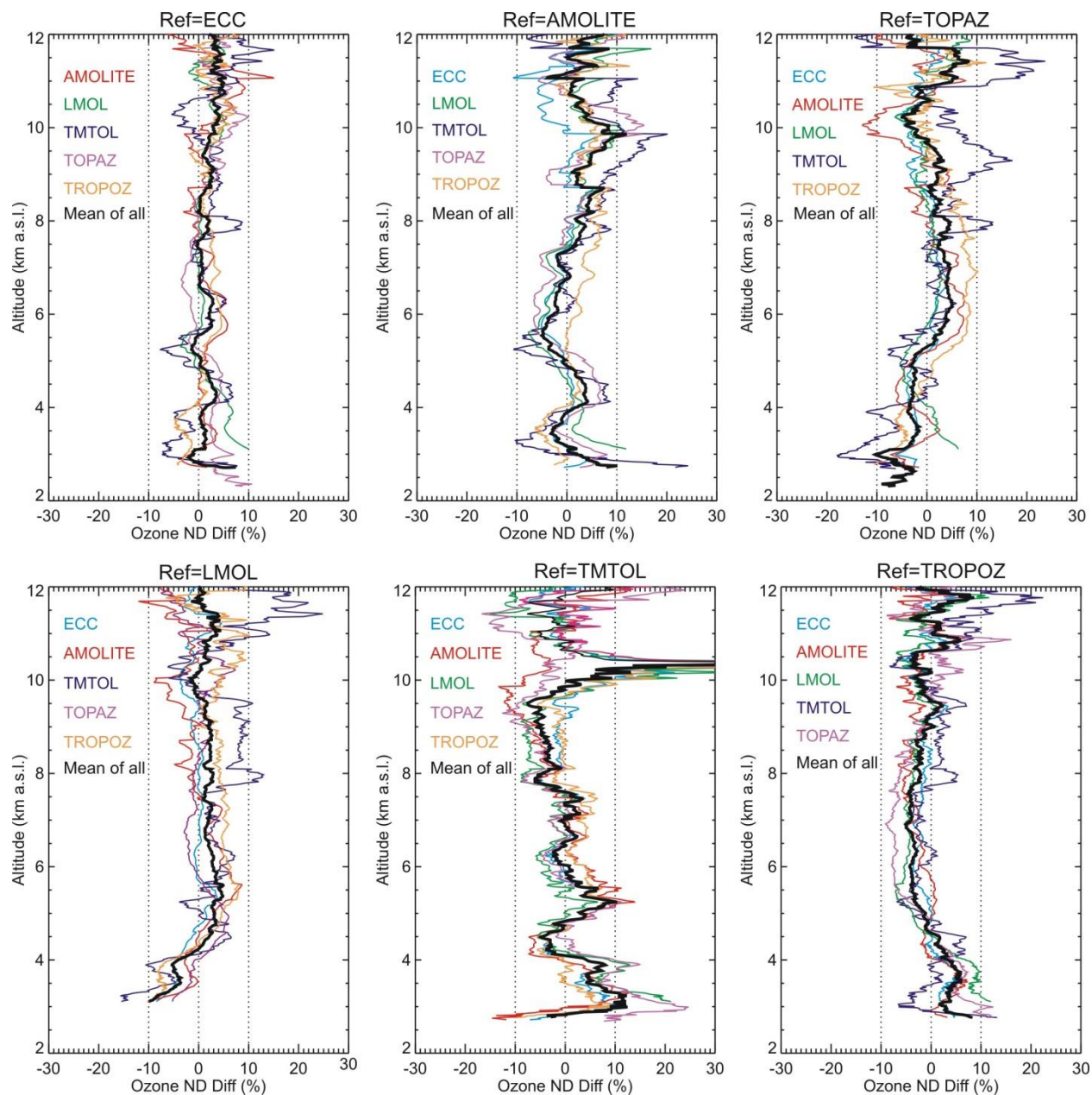
Figure 10: Mean ozone difference (%) between one instrument (referenced on top of each panel) and all the others, computed using all available one-on-one instrument coincidences. Colored curves: one-on-one differences. Black thick curves: Mean of all colored curves.
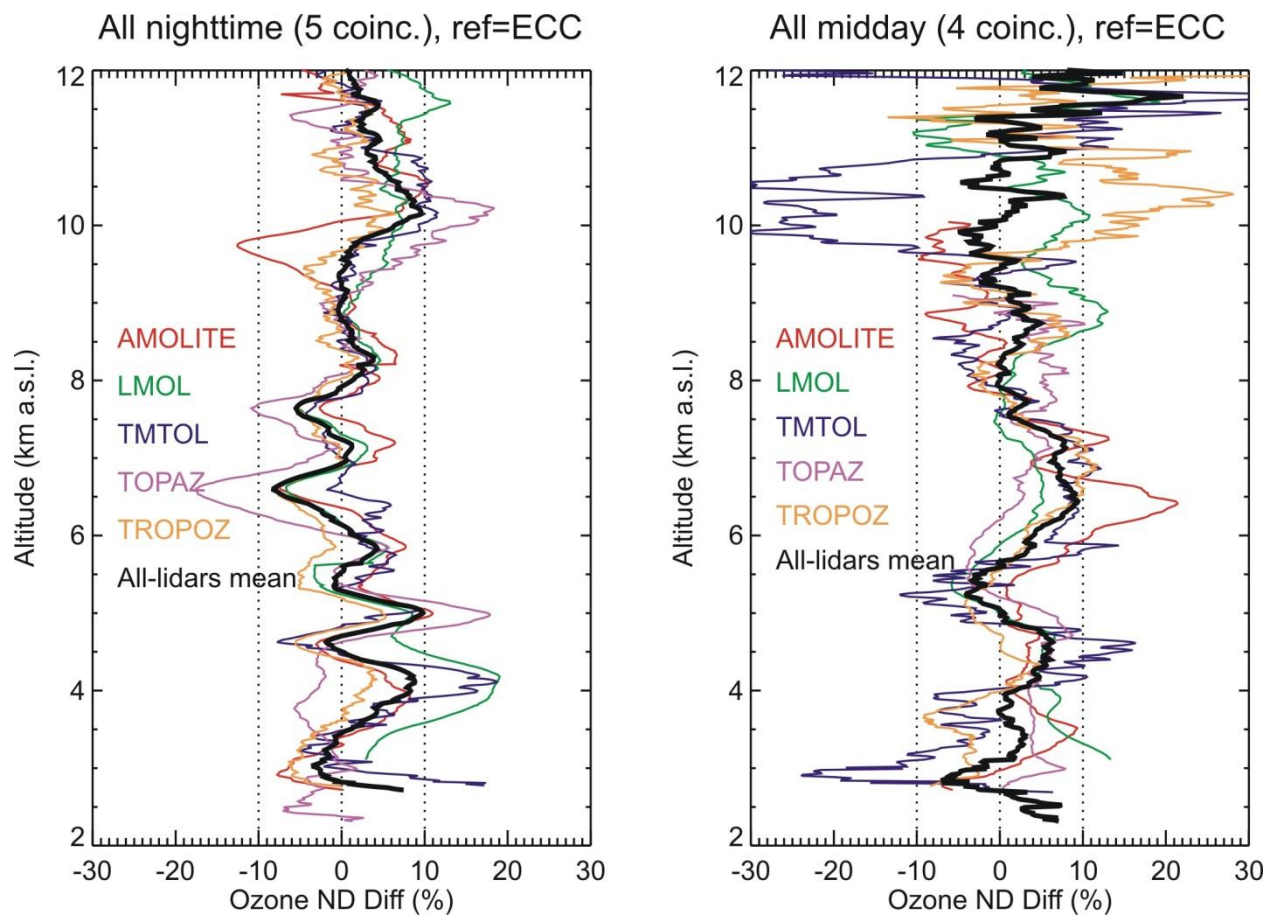
Figure 11: Same as figure 10 top-left panel, but considering only night-time measurements (left panel) and mid-day measurements (right panel).
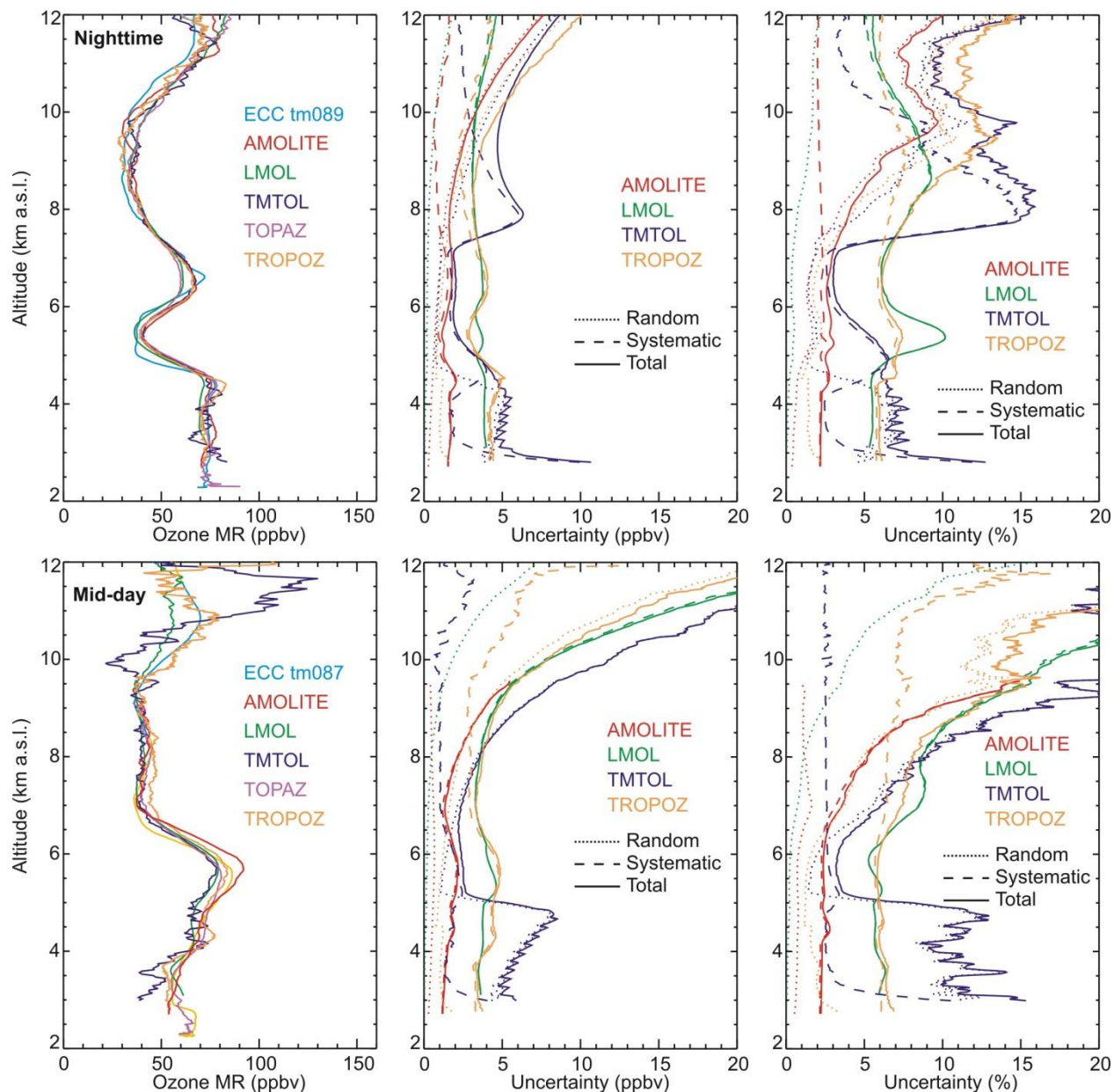
Figure 12: Left panels: Two selected 30-minute ozone profiles measured simultaneously by all five lidars in dark conditions (top) and in the brightest possible daytime conditions (bottom). Middle panels: Ozone uncertainty (in ppbv) associated with the profiles shown on the left panels. Right panels: same as middle panels but expressed in percent. For the uncertainty plots, dotted curves denote the random component, dash curves denote the systematic component, and solid curves denote the total uncertainty.
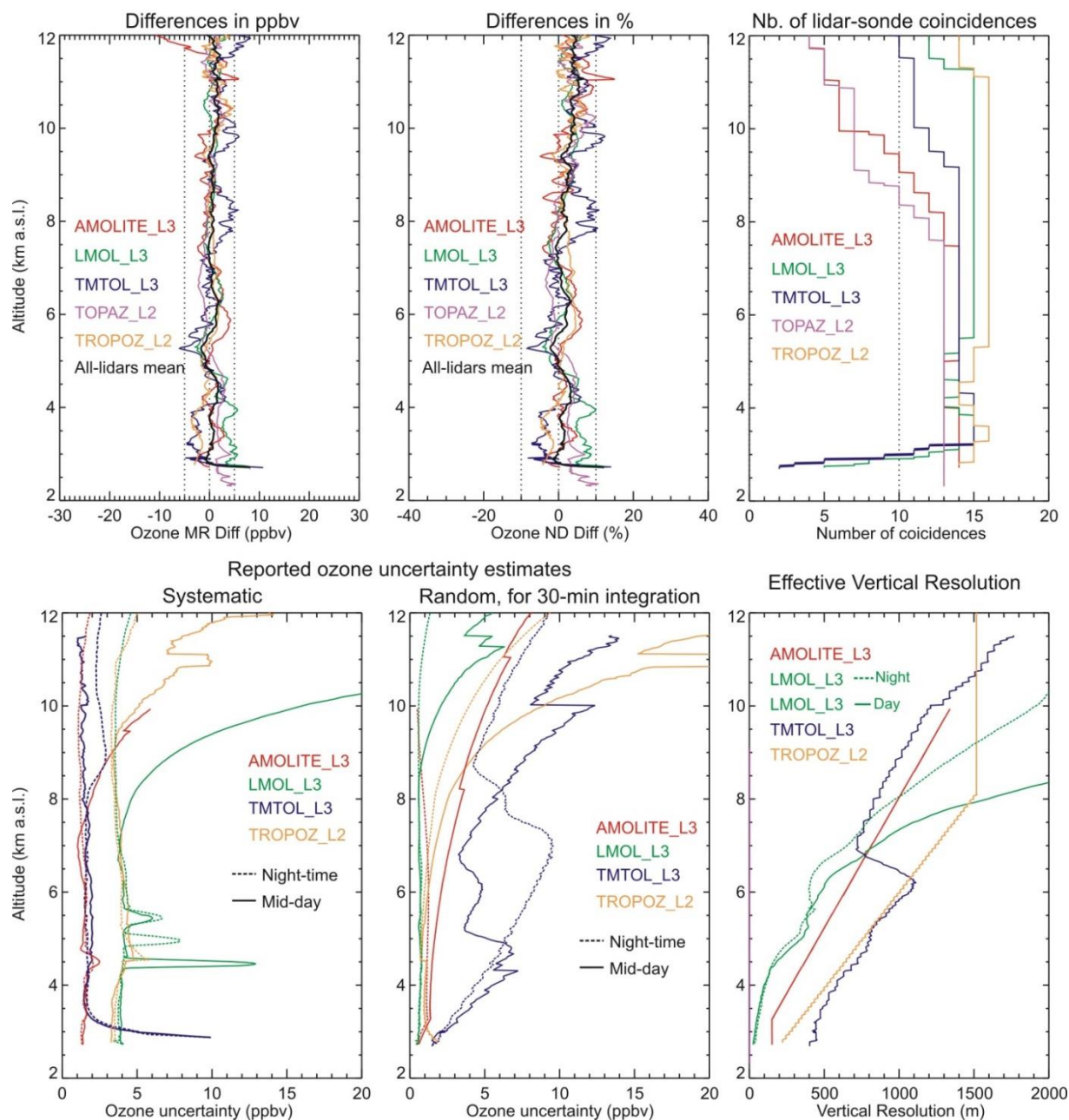
Figure 13: Top-left panel: Mean ozone differences (in ppbv) between the SCOOP Level 3 lidar data (or Level 2 if Level 3 is not available) and ozonesonde, computed using all available one-on-one coincidences during SCOOP. **Top-row, middle panel:** Same as top-left panel, but ozone differences in percent. **Top-right panel:** Number of coincidences used to compute the mean differences. **Bottom-left panel:** Mean of reported systematic uncertainties. Solid curves are during brightest daytime conditions, dash-curves are for night-time conditions. **Bottom row, middle panel:** Same as left panel, but for random uncertainties for 30-min data acquisition. **Bottom-right panel:** Reported effective vertical resolution.
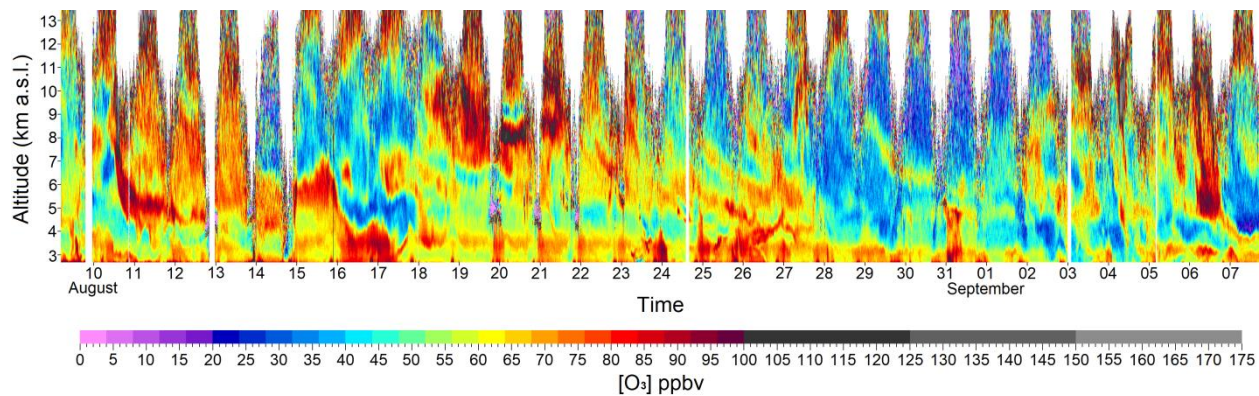
Figure 14: 31-day ozone time-altitude cross-section obtained at TMF by the AMOLITE lidar during - and immediately after - the SCOOP campaign.